Mineralogical Magazine (2022), **86**, 799–813
doi:10.1180/mgm.2022.49

CAMBRIDGE UNIVERSITY PRESS

Article

Mineralogy of the Marepalli lamproite dyke from the Nalgonda district, Telangana, Southern India

Jaspreet Saini[1], Parminder Kaur[1], Roger H. Mitchell[2] and Gurmeet Kaur[1]*

[1]Department of Geology, Panjab University, Chandigarh, India 160014; and [2]Department of Geology, Lakehead University, Thunder Bay Ontario, Canada P7B 5E1

Abstract

The Marepalli dyke of the Vattikod cluster of the Ramadugu Lamproite Field, Nalgonda district, Telangana, India consists of pseudomorphed leucite, phlogopite (Al-poor, Ti-rich zoned phlogopite micas), pseudomorphed olivine, fluorapatite and Al-poor diopside embedded in groundmass consisting mainly of poikilitic Fe-rich titanian phlogopite and potassic amphibole. Other groundmass minerals are Al-Na-poor diopside, Al-poor spinels (titanian magnesian chromites to titanian chromites), Sr-rich fluorapatite and late-stage interstitial anhedral crystals of titanite and K-feldspar. The late-stage deuteric minerals present are REE-rich allanite, pyrite, magnetite, chalcopyrite, galena, hydro-zircon, carbonates (calcite, witherite and strontianite), baryte and cryptocrystalline SiO_2. Apatite is an early crystallising phase and is present as inclusions in phlogopite and pyroxene. Phlogopite and amphibole occur as inclusions in titanite and K-feldspar. The compositional trends of phlogopite are of almost constant Al_2O_3 content with FeO_T and TiO_2 enrichment, and are typical of lamproitic micas. The FeO_T enrichment is accompanied additionally by MgO depletion (reflecting $^{VI}Fe^{2+}$ enrichment) from core to rim together with a slight increase in the tetraferric iron component. Diopside is characterised by <0.4 wt.% alumina and <0.6 wt.% sodium contents and exhibits typical lamproitic affinity. The spinels are alumina-poor with un-evolved titanian magnesian chromite to titanian chromite compositions. The presence of K-richterite, as an abundant amphibole, indicates a lamproite affinity, and on the basis of the typomorphic mineralogy, this rock is classified as a 'pseudoleucite-amphibole-phlogopite lamproite'. The Marepalli lamproite shows significant difference in compositional ranges of phlogopite, amphibole, pyroxene and spinel in comparison to those reported from the Vattikod, Gundrapalli, Ramadugu, Somavarigudem and Yacharam lamproites of Ramadugu Lamproite Field. These lamproites are considered to form from a common parent magma under reducing conditions as evidenced from: (1) low tetraferric iron content in phlogopite; (2) low Fe^{3+}# and Ti# in spinels; and (3) high F content in phlogopite and apatite.

Keywords: lamproite, mineralogy, phlogopite, spinel, Marepalli, Vattikod, Eastern Dharwar Craton

(Received 8 November 2021; accepted 6 May 2022; Accepted Manuscript published online: 22 June 2022; Associate Editor: Leone Melluso)

Introduction

Lamproites are ultrapotassic, volatile rich (dominantly H_2O) peralkaline igneous rocks. These rocks are characterised by complex mineralogy and can be classified using 'mineralogical-genetic classification' schemes (Mitchell and Bergman, 1991; Scott Smith *et al.*, 2018; Mitchell, 2020a). Identification of the typomorphic mineral assemblage is essential for accurate classification and nomenclature of exotic rock types such as lamproites, kimberlites and lamprophyres (Mitchell and Bergman, 1991; Mitchell, 1994, 1995; Tappe *et al.*, 2005; Dongre and Tappe, 2019; Mitchell, 2020a). Lamproites, unlike other common igneous rocks, cannot be classified on the basis of their modal mineralogy. Lamproites occur in anorogenic (cratonic) and orogenic (subduction) tectonic environments (Prelević *et al.*, 2008; Mitchell, 2020b). According to Murphy *et al.* (2002) and Chakrabarti *et al.* (2007), the sublithospheric mantle is the source of lamproites and 'orangeites' however lamproite magmas are generated by the partial melting of sub-continental lithospheric mantle and in some instances are diamondiferous (Mitchell and Bergman, 1991; Scott Smith *et al.*, 2018; Dongre and Tappe, 2019; Mitchell, 2020a; Pandey and Chalapathi Rao, 2020; Krmíček *et al.*, 2022).

Kimberlites (or para-kimberlites), lamproites and ultramafic lamprophyres are considered to be present in close proximity in the Eastern Dharwar Craton (Shaikh *et al.*, 2019). Many of the rocks previously regarded as kimberlites have been reclassified as *bona fide* lamproites on the basis of 'mineralogical-genetic classification' schemes (Fareeduddin and Mitchell, 2012; Gurmeet Kaur *et al.*, 2013; Gurmeet Kaur and Mitchell, 2013, 2016; Shaikh *et al.*, 2017, 2018, 2019). The present work describes the petrography and mineral compositional data for the Marepalli dyke from the Mesoproterozoic Ramadugu Lamproite Field in the Eastern Dharwar Craton, South India.

Geological setting

The Dharwar Craton is divided into the Eastern Dharwar Craton and the Western Dharwar Craton by the Chitradurga Boundary Fault (Naqvi and Rogers, 1987; Swaminath and Ramakrishnan, 1981). The Eastern Dharwar Craton comprises the Late-Archaean granitoids, schist belts and the tonalitic-trondhjemite-granodiorite

*Author for correspondence: Gurmeet Kaur, Email: gurmeet28374@yahoo.co.in
Cite this article: Saini J., Kaur P., Mitchell R.H. and Kaur G. (2022) Mineralogy of the Marepalli lamproite dyke from the Nalgonda district, Telangana, Southern India. *Mineralogical Magazine* **86**, 799–813. https://doi.org/10.1180/mgm.2022.49

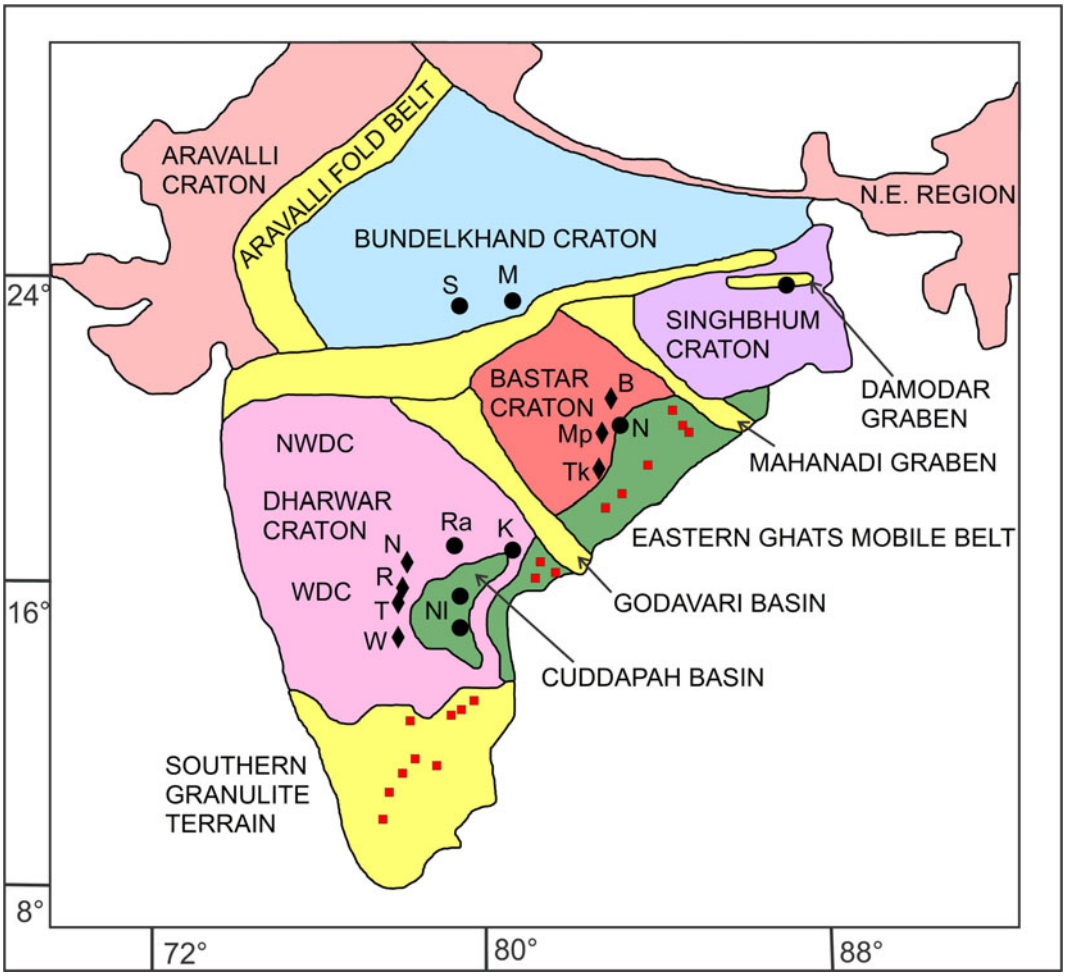

Fig. 1. Distribution of lamproites (black circles: S – Saptarshi; M – Majhgawan; D – Damodar; Na – Nawapara; Ra – Ramadugu; K – Krishna; NI – Nallamalai–Chelima) and lamproite–kimberlite fields (black labeled diamonds: B – Basna; Mp – Mainpur; Tk – Tokopal; N – Narayanpet; R – Raichur; T – Tungabhadra; W – Wajrakarur) in the cratons of the Indian subcontinent together with the locations of deformed Proterozoic alkaline rocks and carbonatites (red squares) in the Eastern Ghats Mobile Belt and Southern Granulite Terrain (after Gurmeet Kaur *et al.*, 2018; Mitchell, 2020b).

gneiss of the Peninsular Gneissic Complex. The Peninsular Gneissic Complex is overlain by the Proterozoic Sedimentary Cuddapah basin, covering the eastern part of the Eastern Dharwar Craton (Ramakrishnan and Vaidyanadhan, 2008; Jayananda *et al.*, 2018). The Archaean rocks of the Eastern Dharwar Craton are further intruded by the Paleoproterozoic mafic dykes, Mesoproterozoic kimberlites and lamproites and calc-alkaline lamprophyres (Kumar *et al.*, 2015; Gurmeet Kaur and Mitchell, 2013, 2016; Gurmeet Kaur *et al.*, 2013; Srivastava *et al.*, 2015; Shaikh *et al.*, 2017, 2018, 2019; Chalapathi Rao *et al.*, 2020). The lamproite fields of Eastern Dharwar Craton present in the Cuddapah Basin are: the Banganapalle Lamproite Field (Garledinne); the Nallamalai Lamproite Field (Chelima and Zangamarajupalle); and the Somasila Lamproite Field (Sridhar and Rau, 2005; Kumar *et al.*, 2013; Ahmed *et al.*, 2016). These are grouped as the Cuddapah Basin lamproites. The Ramadugu Lamproite Field and Krishna Lamproite Field occur along the northwestern and northeastern margins of the Cuddapah Basin, respectively (Fig. 1; Gurmeet Kaur *et al.*, 2018; Chalapathi Rao *et al.*, 2010; Talukdar *et al.*, 2018; Shaikh *et al.*, 2019). The recent studies on the reclassification of P-2 west, P-4, P-5, P-12, P-13, TK-1 and TK-4 kimberlites from the Wajrakarur Kimberlite Field in the Eastern Dharwar Craton as lamproites by Gurmeet Kaur and Mitchell (2013, 2016), Gurmeet Kaur *et al.* (2013) and Shaikh *et al.* (2017, 2018, 2019) are significant in unravelling the nature of these rocks. The Ramadugu Lamproite Field consists of lamproites dykes named after the local villages and includes: Ramadugu; Somavarigudem; Yacharam; Vattikod; Gundrapalli; and Marepalli (Fig. 2; Kumar *et al.*, 2013; Chalapathi Rao *et al.*, 2014; Gurmeet Kaur *et al.*, 2018; Gurmeet Kaur and Mitchell, 2019). The lamproites of Krishna, Nallamalai and Ramadugu lamproite fields are diamondiferous. The para-kimberlites and lamproites of Eastern Dharwar Craton are poorly diamondiferous (e.g. < 2 carats per hundred tons for the Wajrakarur Lamproite Field) however the diamonds are of gem quality, as reported by Ravi *et al.* (2013). The Ramadugu and Krishna lamproites are non-prospective, i.e. diamonds with no commercial value (Chalapathi Rao *et al.*, 2014).

Marepalli dyke

The Marepalli lamproite dyke was first recognised by Kumar *et al.* (2013) as part of the Vattikod lamproite cluster in the Ramadugu Lamproite Field (Fig. 2). The dyke occurs 1.5 km west of the Marepalli village (16°53′00.8″N, 79°02′38.6″E) and intrudes the migmatitic gneiss unit of the Peninsular Gneissic Complex

https://doi.org/10.1180/mgm.2022.49 Published online by Cambridge University Press

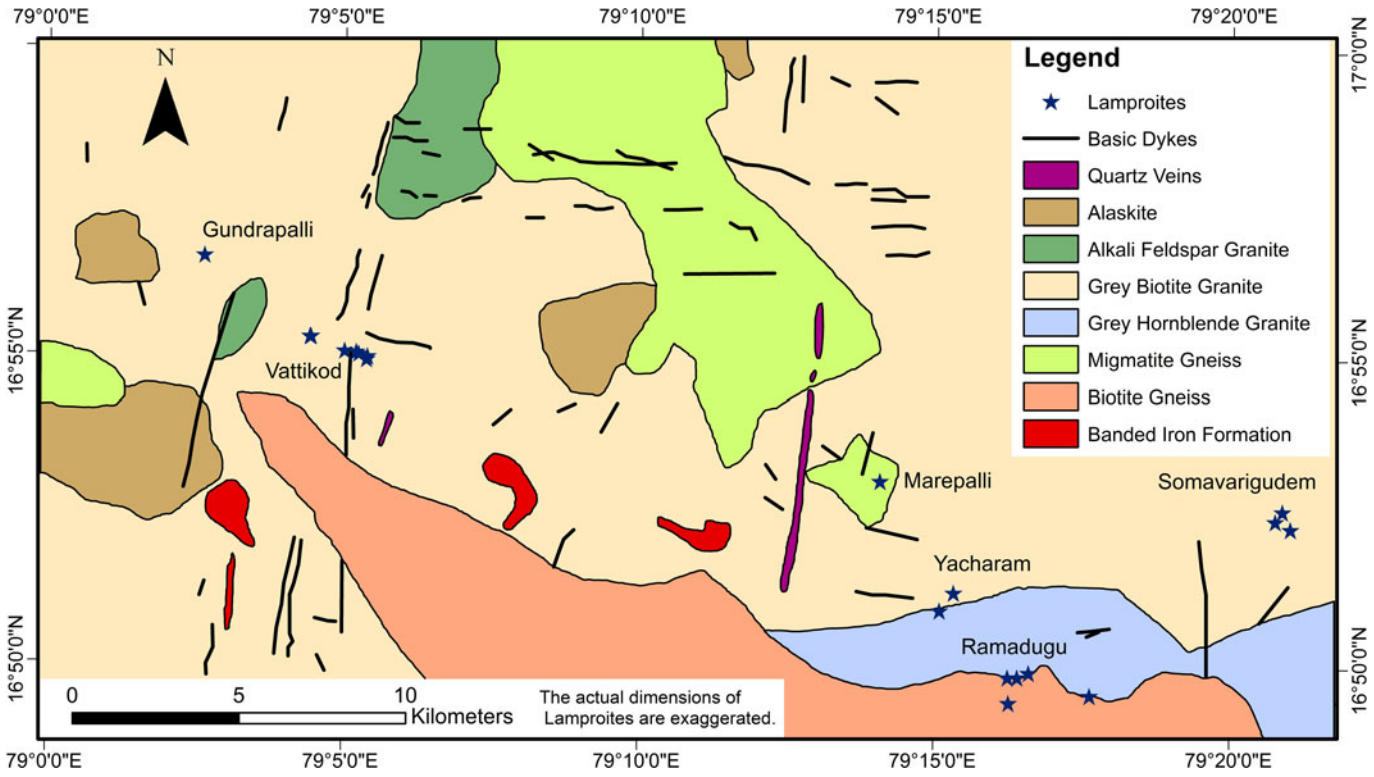

Fig. 2. Geological map showing the lamproitic intrusions in Ramadugu Lamproite Field (compiled from Kumar *et al.*, 2013 and Sridhar and Rau, 2005).

along the fractures in a NW–SE direction (Kumar *et al.*, 2013; Talukdar *et al.*, 2018). On the basis of a 'mineralogical-genetic classification' scheme, the Marepalli dyke is a *bona fide* pseudoleucite-amphibole-phlogopite lamproite. The mineralogical characteristics of the Marepalli dyke are compared with those of the neighbouring Vattikod cluster and Gundrapalli lamproite dyke lying to the northwest, and the Ramadugu, Somavarigudem and Yacharam lamproite dykes in the southeast, which together form part of the Ramadugu Lamproite Field.

Analytical techniques

Representative samples from the Marepalli dyke were investigated by quantitative energy-dispersive X-ray spectrometry using a Hitachi SU-70 scanning electron microscope at Lakehead University, Ontario, Canada. The raw X-ray data were obtained with a beam current of 300 pA, an accelerating voltage of 20 kV and 30–60 s counting times and processed using Oxford *AZtec* software. For information regarding the standards used, refer to Liferovich and Mitchell (2005).

Petrography of the Marepalli dyke

The Marepalli dyke is a greenish black and fine-grained rock (Fig. 3a). Petrographic studies reveal that it is inequigranular in texture with variable sized microphenocrysts and groundmass phases. The rock is characterised by the presence of microphenocrysts of rounded–subrounded pseudomorphed leucite and mica as the principle phases, together with euhedral-to-subhedral pseudomorphed olivine, apatite and clinopyroxene. These microphenocrysts are embedded in a fine-grained groundmass of mica, apatite, clinopyroxene, spinel, amphibole, titanite, K-feldspar and calcite with quartz being the final crystallising interstitial mineral (Figs 3b–c, 4a–d).

Rounded-to-subrounded microphenocrysts of leucite are completely pseudomorphed by secondary K-feldspar intergrown with calcite, quartz, cryptocrystalline silica, and contain small inclusions of allanite, pyrite, magnetite, chalcopyrite, galena, titanite and hydro-zircon. Fresh olivine is not found, although it occurs as euhedral-to-subhedral pseudomorphs of calcite surrounded by microphenocrysts of anthophyllite and phlogopite at the margins (Fig. 4a). In contrast, mica, apatite and clinopyroxene occur as alteration-free primary microphenocrysts. Mica is the most abundant phase and is present as zoned microphenocrysts with compositionally distinct cores and rims. Mica also occurs as zonation-free groundmass grains and is present in the marginal part of olivine pseudomorphs (Fig. 4a). Apatite is the second common primary phase, and occurs texturally as two types: (1) euhedral-to-subhedral acicular microphenocrysts (Fig. 4c); and (2) tiny hexagonal prisms scattered throughout the rock. Apatite prisms and microphenocrysts are also completely- or partially-enclosed by mica and clinopyroxene microphenocrysts, indicative of their earlier crystallisation. The majority of apatites are not zoned, although compositional zoning is observed in one microphenocryst partially-included in clinopyroxene. Marepalli clinopyroxene is commonly present as zonation-free microphenocrysts and in the groundmass, unlike those reported from the Vattikod and Gundrapalli lamproites (Fig. 4c; Gurmeet Kaur *et al.*, 2018; Talukdar *et al.*, 2018; Gurmeet Kaur and Mitchell, 2019). Most clinopyroxene in the Marepalli dyke are corroded and commonly replaced by titanite along the grain margins and cracks.

Spinels occur as tiny euhedral crystals scattered throughout the groundmass and are also present along the margins of olivine

https://doi.org/10.1180/mgm.2022.49 Published online by Cambridge University Press

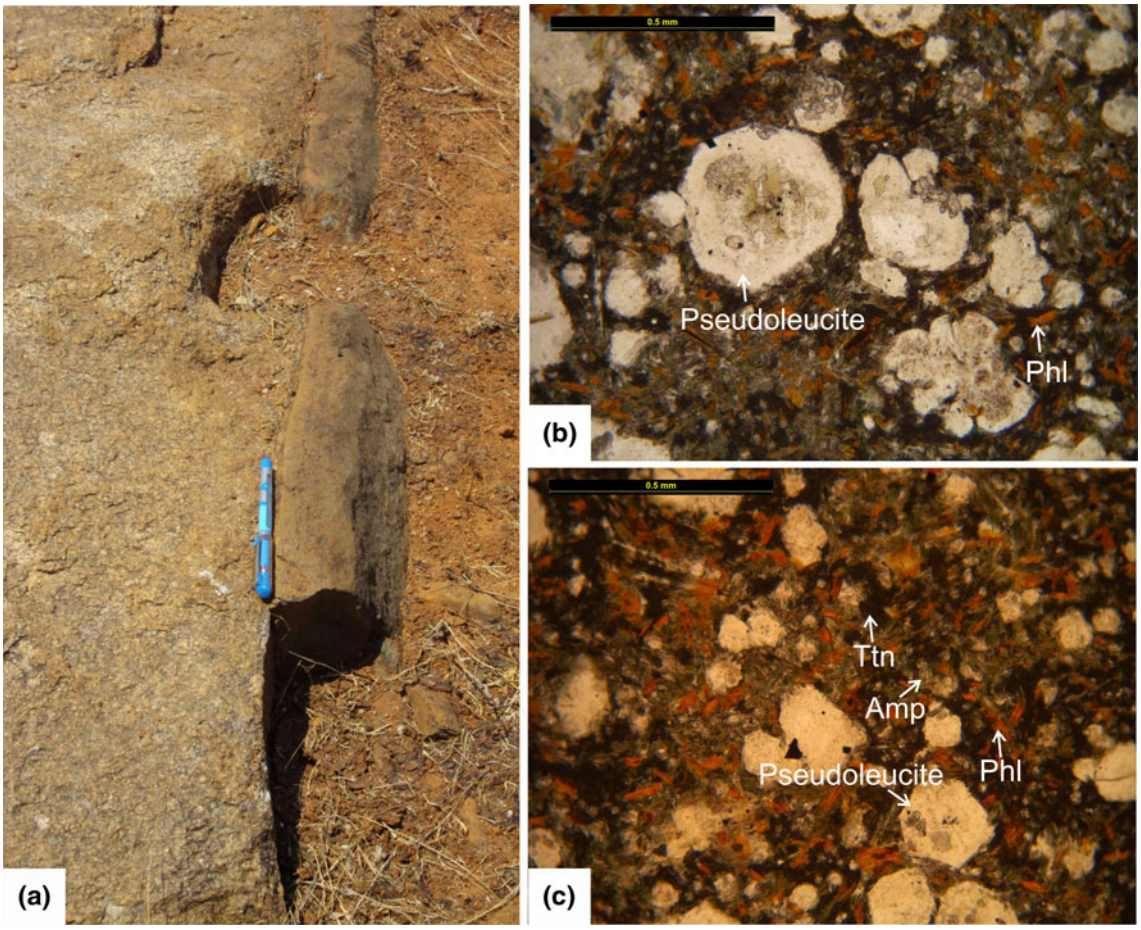

Fig. 3. (a) Field photograph showing an outcrop of the Marepalli lamproite dyke intruding the Peninsular Gneissic Complex; (b) and (c) plane-polarised light images showing the inequigranular texture of the Marepalli lamproite dyke rock with ovoid pseudoleucites, reddish-brown elongated phlogopite (Phl) microphenocrysts in a fine-grained groundmass of greenish-brown prismatic amphibole (Amp), dark brown titanite (Ttn) and phlogopite (Phl).

pseudomorphs (Fig. 4c). Spinels occasionally show compositional zoning identified as core surrounded by a weakly developed thin rim. Amphiboles essentially occur as subhedral-to-anhedral groundmass crystals in association with fine-grained phlogopite, spinel, apatite and titanite (Fig. 4d). Subhedral amphibole crystals exhibit compositional zoning and are commonly enclosed by titanite aggregates in the groundmass (Fig. 4b). Titanite occurs in three different parageneses: (1) dominantly as late-stage primary phase aggregates containing inclusions of mica, apatite, pyroxene and amphibole (Fig. 4b); (2) a secondary phase replacing clinopyroxene along the grain boundaries, cleavage planes and fractures; and (3) along the margins of leucite pseudomorphs. The feldspars are commonly present as primary anhedral poikilitic crystals occupying the interstitial spaces in the groundmass and as the principle secondary phase pseudomorphing leucite (Fig. 4a–d). Calcite occurs as: (1) a late-stage deuteric phase filling the interstices between earlier-formed groundmass phases; and (2) a secondary phase together with K-feldspar and quartz in the leucite pseudomorphs (Fig 4a). Similar calcite has been recorded in the Vattikod and Gundrapalli lamproites (Gurmeet Kaur *et al.*, 2018; Talukdar *et al.*, 2018; Gurmeet Kaur and Mitchell, 2019). The textural features of accessory phases (allanite; hydro-zircon; pyrite; magnetite; chalcopyrite; galena; witherite; strontianite; baryte; chlorite; and serpentine) indicate their late secondary occurrence as a result of late-stage deuteric or post-magmatic hydrothermal alteration. Allanite and hydro-zircon occur as fine-grained aggregates in the core of leucite pseudomorphs. Magnetite and pyrite are observed as anhedral crystals within leucite pseudomorphs. Rare anhedral galena and Co–Ni-chalcopyrite are present in the olivine pseudomorphs. Witherite and strontianite are rarely present in the groundmass. Baryte is observed as veins cross-cutting the rock. Minor chlorite and serpentine occur as alteration products. Chlorite rarely replaces groundmass phlogopite, pyroxene and amphibole, and rare serpentine is present as pseudomorphs after former subhedral olivine.

Mineral compositions

Mica

Representative compositions of mica are given in Table 1. Marepalli micas occurring as microphenocrysts and groundmass phase are phlogopites with X_{Mg} [the ratio $Mg/(Mg+Fe^{2+})$] in the range of 0.92–0.67 (Fig. 5). There is marked difference in FeO_T and TiO_2 in the cores and rims of these zoned phlogopite microphenocrysts, however, Al_2O_3 show overlapping concentrations on Al_2O_3 *vs.* FeO_T and Al_2O_3 *vs.* TiO_2 compositional variation plots (Fig. 6a–b). The cores contain 7.7–6.7 wt.% Al_2O_3, 19.4–21.2 wt.% MgO, 8.7–9.7 wt.% FeO_T and 6.4–6.7 wt.%

https://doi.org/10.1180/mgm.2022.49 Published online by Cambridge University Press

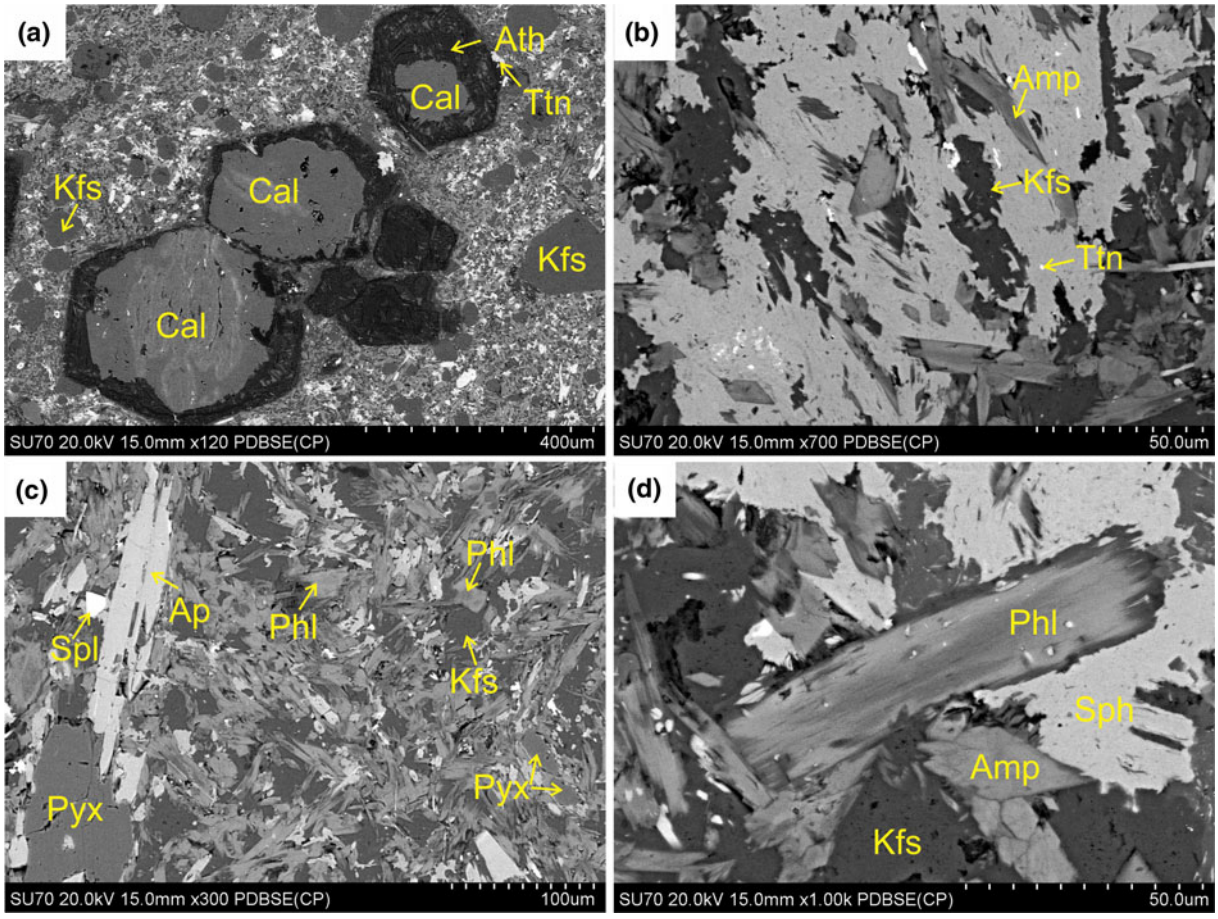

Fig. 4. Back-scattered electron (BSE) images. (a) Euhedral olivine phenocrysts pseudomorphed by secondary calcite (Cal) in the core and anthophyllite (Ath), phlogopite (Phl) and titanite (Ttn) in the rim. Also seen are anhedral leucite phenocrysts completely pseudomorphed by secondary K-feldspar (Kfs). (b) Prismatic amphibole (Amp), aggregates of titanites (Ttn) and K-feldspar (Kfs) as groundmass phases. (c) Phenocrysts of apatite (Ap) and pyroxene (Pyx) in a fine grained groundmass of phlogopite (Phl), K-feldpsar (Kfs), pyroxene (Pyx) and spinel (Spl). (d) Zoned microphenocryst of phlogopite (Phl) in groundmass of amphibole (Amp), titanite (Ttn) and K-feldspar (Kfs).

TiO_2, whereas the rims are characterised by overlapping Al_2O_3 (5.2–7.1 wt.%), relatively decreased MgO (14.1–18.1 wt.%), highly enriched FeO_T (13.6–17.8 wt.%) and slightly increased TiO_2 (6.5–8.1wt.%). The groundmass phlogopites have similar compositions to the rims of the zoned phlogopite microphenocrysts in terms of their Al_2O_3 (7–8.3 wt.%), MgO (14.9–15.9 wt.%), FeO_T (16.3–17.6 wt.%) and TiO_2 (5.9–6.4 wt.%) content. The compositional evolution observed in the Marepalli phlogopites is towards $^{VI}Fe^{2+}$ enrichment, compensated by significant substitution of $^{VI}Mg^{2+}$ by $^{VI}Fe^{2+}$ at the octahedral-site (Table 1). The phlogopite also shows a minor component of stoichiometrically recalculated tetraferric iron (0.48–0.89 atoms per formula unit), suggestive of slight substitution of $^{IV}Al^{3+}$ by $^{IV}Fe^{3+}$ at the tetrahedral site. The high X_{mg} (0.88–0.92) observed in cores of zoned phlogopite microphenocrysts indicates their early crystallisation from less evolved lamproitic melt (Mitchell and Bergman, 1991). However, the rims of zoned phlogopite microphenocrysts and groundmass grains showing relatively low and wider range of X_{mg} (0.67–0.81) are considered to be formed at a late-stage in equilibrium with the evolving magma (Mitchell and Bergman, 1991). The mica occurring at the marginal parts of the olivine pseudomorph are also phlogopites with 0.74–0.75 X_{mg} (Fig. 5). These phlogopites are characterised by high Al_2O_3 (10.4–10.9 wt.%), MgO (20.9–20.3 wt.%), moderate FeO_T (12.6–12.2 wt.%), very low Cr_2O_3 (0.2–0.3 wt.%), NiO (0.2 wt.%) and negligible TiO_2. The composition and textural characteristics of these phlogopites are indicative of their crystallisation prior to phenocrystal phlogopites, at mantle depths (Mitchell and Bergman, 1991). The BaO contents in all textural types of phlogopites are typically <1.6 wt.% and fluorine contents vary between 0–1.2 wt.%.

Mica compositional zonation trends are similar to those found in *bona fide* lamproites (Mitchell and Bergman, 1991; Mitchell, 2020a) and are unlike the trends shown by minettes and archetypal kimberlites (Fig. 6a–b). The compositions of Marepalli mica determined in this work are in agreement with those reported previously from the Vattikod and Gundrapalli lamproites (Figs 5, 6a–b; Gurmeet Kaur *et al.*, 2018; Gurmeet Kaur and Mitchell, 2019). However, the Marepalli mica is more evolved than mica occurring in the Ramadugu, Somavarigudem and Yacharam lamproites and less evolved than that in the Vattikod and Gundrapalli lamproites in terms of Al_2O_3 and FeO_T content (Fig. 6a; Chalapathi Rao *et al.*, 2014; Gurmeet Kaur *et al.*, 2018; Gurmeet Kaur and Mitchell, 2019).

Amphiboles

Representative compositions of Marepalli amphiboles are given in Table 2. Although a wide compositional variation exists, all amphiboles are depleted in Al_2O_3 (<0.7 wt.%) and enriched in

https://doi.org/10.1180/mgm.2022.49 Published online by Cambridge University Press

Table 1. Representative compositions (wt.%) of phlogopite.

Main element oxides	1C	1R	2C	2R	3	4	5	6	7	8	9C	9R	10C	10R	11C	11R	12	13	14
Wt.%																			
SiO_2	41.54	41.38	41.68	38.39	41.09	40.43	41.62	39.67	40.96	40.39	40.97	39.60	40.88	41.78	40.73	40.02	45.57	46.44	44.79
TiO_2	6.35	6.45	6.53	6.92	5.92	6.43	6.13	6.25	6.15	5.86	6.68	7.02	6.60	8.10	6.53	6.78	n.d.	n.d.	n.d.
Al_2O_3	7.61	6.55	6.82	5.45	8.31	7.07	7.30	7.30	7.02	7.96	7.66	7.09	6.72	5.19	7.48	6.78	10.93	10.40	10.63
Cr_2O_3	n.d.	n.d.	n.d.	n.d.	n.d.	n.d.	n.d.	n.d.	n.d.	n.d.	n.d.	n.d.	n.d.	n.d.	n.d.	n.d.	0.26	0.24	0.26
FeO*	8.71	13.60	9.72	17.77	17.24	17.51	16.32	16.42	17.56	17.11	8.90	15.74	9.29	15.75	9.58	16.59	12.59	12.15	12.57
MnO	n.d.	n.d.	n.d.	n.d.	n.d.	n.d.	n.d.	0.18	0.25	n.d.	n.d.	n.d.	n.d.	n.d.	n.d.	n.d.	n.d.	n.d.	n.d.
MgO	21.21	18.10	20.52	14.11	15.10	14.99	15.49	14.89	15.08	15.88	20.02	15.26	20.42	15.05	19.36	14.85	20.56	20.94	20.31
K_2O	9.80	9.43	9.65	8.51	9.10	9.27	8.89	9.09	8.06	8.76	9.36	9.00	9.96	9.63	8.91	9.37	8.66	8.86	9.13
BaO	1.47	1.55	1.44	1.46	0.97	1.03	0.94	1.01	0.95	1.07	1.26	1.01	1.32	0.97	1.08	1.31	n.d.	n.d.	n.d.
NiO	n.d.	n.d.	n.d.	n.d.	n.d.	n.d.	n.d.	n.d.	n.d.	n.d.	n.d.	n.d.	n.d.	n.d.	n.d.	n.d.	n.d.	0.24	0.23
F	1.07	0.97	1.04	0.41	0.49	0.93	0.48	n.d.	n.d.	n.d.	0.96	0.63	0.79	0.89	1.11	0.65	0.61	1.14	1.10
Analytical sum	96.69	97.06	96.36	92.61	97.73	96.73	96.69	94.81	96.03	97.03	94.85	94.72	95.19	96.47	93.67	95.70	98.57	99.27	97.92
Structural formula calculated on the basis of 22 atoms of oxygen																			
Si	6.020	6.109	6.086	6.088	6.072	6.078	6.181	6.064	6.152	6.018	6.038	6.036	6.050	6.251	6.076	6.084	6.366	6.435	6.338
^{IV}Al	1.300	1.140	1.174	1.019	1.447	1.253	1.278	1.315	1.243	1.398	1.330	1.274	1.172	0.915	1.315	1.215	1.634	1.565	1.662
Fe^{3+}	0.681	0.751	0.741	0.893	0.481	0.669	0.542	0.621	0.605	0.584	0.632	0.691	0.778	0.834	0.609	0.702	–	–	–
Σ(T site)	8.000	8.000	8.000	8.000	8.000	8.000	8.000	8.000	8.000	8.000	8.000	8.000	8.000	8.000	8.000	8.000	8.000	8.000	8.000
^{VI}Al	–	–	–	–	–	–	–	–	–	–	–	–	–	–	–	–	0.166	0.133	0.110
Ti	0.692	0.716	0.717	0.825	0.658	0.727	0.685	0.718	0.695	0.657	0.740	0.805	0.735	0.911	0.733	0.775	–	–	–
Cr	–	–	–	–	–	–	–	–	–	–	–	–	–	–	–	–	0.029	0.026	0.029
Fe^{2+}	0.375	0.928	0.446	1.464	1.649	1.532	1.485	1.478	1.601	1.548	0.465	1.316	0.372	1.136	0.586	1.407	1.471	1.408	1.487
Mn	–	–	–	–	–	–	–	0.023	0.032	–	–	–	–	–	–	–	–	–	–
Mg	4.582	3.984	4.466	3.336	3.326	3.360	3.429	3.393	3.377	3.527	4.398	3.467	4.505	3.357	4.305	3.365	4.282	4.325	4.284
Ni	–	–	–	–	–	–	–	–	–	–	–	–	–	–	–	–	–	0.027	0.026
Σ(O site)	5.649	5.627	5.629	5.625	5.633	5.619	5.599	5.613	5.704	5.732	5.604	5.588	5.612	5.404	5.623	5.548	5.948	5.920	5.937
Ba	0.083	0.090	0.082	0.091	0.056	0.061	0.055	0.060	0.056	0.062	0.073	0.060	0.077	0.057	0.063	0.078	–	–	–
K	1.812	1.776	1.797	1.722	1.715	1.778	1.684	1.773	1.544	1.665	1.760	1.750	1.881	1.838	1.696	1.817	1.543	1.566	1.648
Σ(X site)	1.895	1.866	1.880	1.813	1.772	1.839	1.739	1.833	1.600	1.728	1.833	1.810	1.957	1.895	1.759	1.895	1.543	1.566	1.648
All cations	16.035	15.946	15.990	15.643	15.634	15.900	15.563	15.446	15.304	15.459	15.884	15.702	15.939	15.720	15.906	15.755	15.761	15.999	16.078
Mg#	0.92	0.81	0.91	0.70	0.67	0.69	0.70	0.70	0.68	0.70	0.90	0.72	0.92	0.75	0.88	0.71	0.74	0.75	0.74

n.d. – not detected; FeO* – total Fe expressed as FeO; C – Core and R – Rim; Mg# = Mg/(Mg+Fe^{2+})
Compositions: 1–2, 9–11, microphenocrysts; 3–8, groundmass; 12–14, included in olivine pseudomorphs at rims.

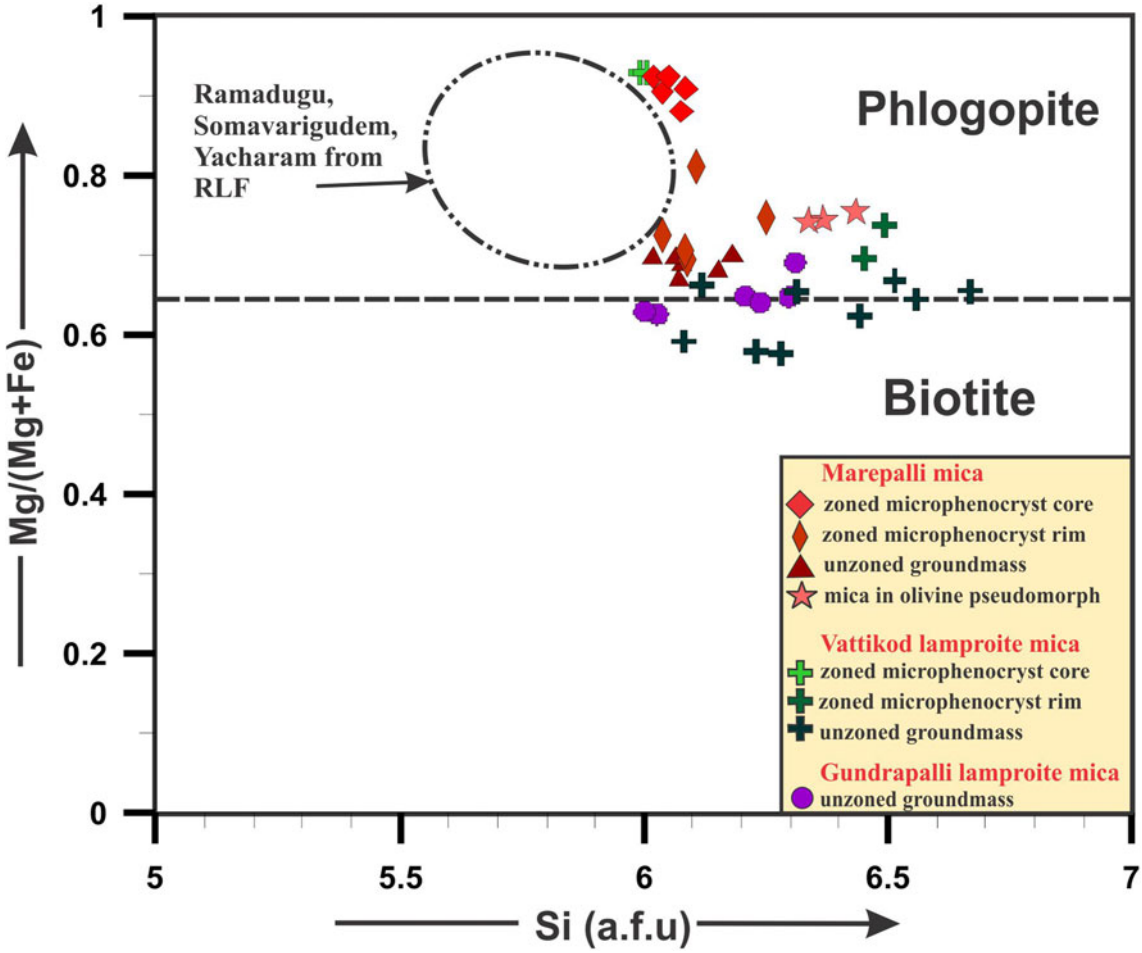

Fig. 5. Mg# *vs.* Si (a.f.u = atoms per formula unit) classification diagram for mica compositions (after Rieder *et al.*, 1998). Also shown are data for the micas from Vattikod (Gurmeet Kaur *et al.*, 2018) and Gundrapalli (Gurmeet Kaur and Mitchell, 2019) lamproites and the field for other Ramadugu lamproites (Chalapathi Rao *et al.*, 2014).

TiO_2 (2–5.1 wt.%), and thus typical of most lamproitic amphiboles crystallising from a peralkaline magma (Mitchell and Bergman, 1991). The overall compositional range of Marepalli amphibole is 4.4–6 wt.% Na_2O, 1.6–5.5 wt.% K_2O, 11.6–23.7 wt.% FeO_T, 0.54–15.1 wt.% MgO and 2.7–5.3 wt.% CaO. These amphiboles exhibit an exceptionally wide compositional evolution from titanian potassic-katophorite through potassic-ferro-katophorite, potassic-katophorite, potassic-ferro-richterite and potassic-richterite to titanian potassic-arfvedsonite (Table 2). However, potassic-richterite is predominant. In a FeO_T *vs.* Na_2O compositional variation diagram (Fig. 7a), the Marepalli amphiboles evolve to the compositions that are higher in FeO_T than typical lamproites *sensu lato*, and overlap the compositional trend of amphiboles from the West Kimberley lamproites. The Ti content varies consistently with the essentially constant Na/K ratio in a Ti *vs.* Na/K plot (Fig. 7b). Although most of the compositions lie in none of the fields delineated in the Ti *vs.* Na/K plot, they do show some affinity with those of the Smoky Butte and Leucite Hills lamproites (Fig. 7b). Figures 7a and b demonstrate that the majority of Marepalli amphiboles are similar to those from the Vattikod lamproites (Gurmeet Kaur *et al.*, 2018), and are more evolved than Gundrapalli lamproite (Gurmeet Kaur and Mitchell, 2019). Additionally, the majority of Marepalli amphiboles are also similar to those of Ramadugu, Somavarigudem and Yacharam lamproites, though exhibit a more extensive evolutionary trend (Fig. 7a–b; Chalapathi Rao *et al.*, 2014).

Clinopyroxene

The microphenocrysts and groundmass clinopyroxene in Marepalli are diopsidic in composition with a compositional range of $Wo_{45.6–46.6}En_{47.2–49.0}Fs_{4.6–6.4}$ (Table 3). They have high MgO (17.1–17.9 wt.%) and CaO (22.7–23.6 wt.%) and are extremely depleted in Al_2O_3 (<0.4 wt.%), with low TiO_2 (1.2–2.2 wt.%), $FeO_{(T)}$ (2.9–4.1 wt.%), Na_2O (<0.6 wt.%) and Cr_2O_3 (<1.0 wt.%), indicating they are a diopside of uniform composition and similar to pyroxenes from lamproites in other localities (Table 3; Mitchell and Bergman, 1991).

The diopsides from Marepalli are similar in composition to those reported previously from the Gundrapalli lamproite, but differ from those in the Vattikod lamproites which contain two distinct varieties of clinopyroxene, i.e. diopside and Na-Fe-rich pyroxenes extremely enriched in $FeO_{(T)}$ (up to 17 wt.%; Gurmeet Kaur *et al.*, 2018; Gurmeet Kaur and Mitchell, 2019). The Ti *vs.* Al (atoms per formula unit) plot of pyroxene compositions shows that all Marepalli clinopyroxenes fall well within the lamproite field and have comparable compositions to those in

https://doi.org/10.1180/mgm.2022.49 Published online by Cambridge University Press

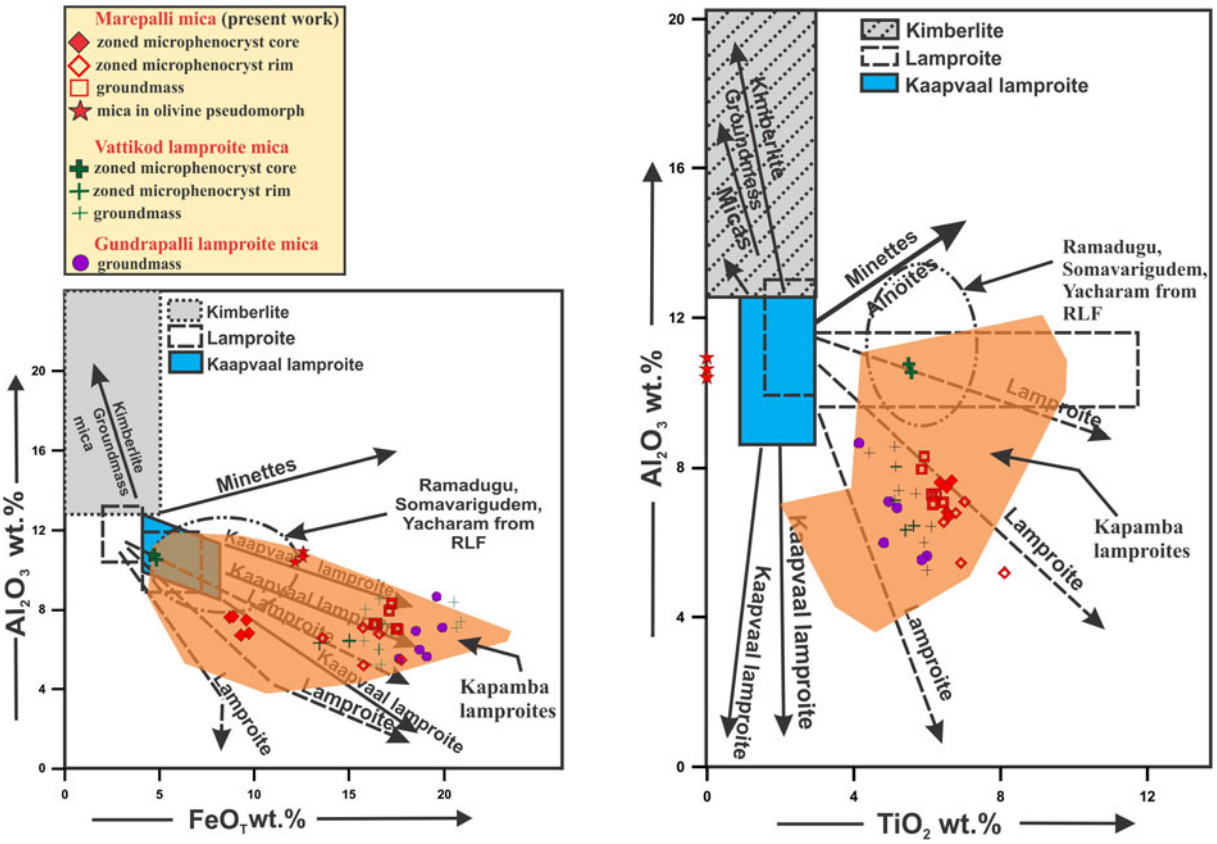

Fig. 6. (a) Al_2O_3 (wt.%) *vs*. FeO_T (wt.%); and (b) Al_2O_3 (wt.%) *vs.* TiO_2 (wt.%) compositional variation diagram of mica in Marepalli lamproite. Also shown are data for the micas from Vattikod (Gurmeet Kaur *et al.*, 2018) and Gundrapalli (Gurmeet Kaur and Mitchell, 2019) lamproites and the field for other Ramadugu lamproites (Chalapathi Rao *et al.*, 2014). The compositional field for mica in Kapamba lamproites is taken from Ngwenya and Tappe (2021). Compositional fields and trends for kimberlites, lamproite, Kaapvaal lamproite (formerly orangeite) and minette micas from Mitchell (1995).

Ramadugu, Somavarigudem and Yacharam lamproites (Fig. 8; Chalapathi Rao *et al.*, 2014). However, Gundrapalli lamproite clinopyroxenes have high TiO_2 (2.8–4.1 wt.%) relative to Marepalli and Vattikod lamproite clinopyroxenes that contain TiO_2 ranging from 1.2–2.2 wt.% and 0.4–2.4 wt.% respectively (Fig. 8; Gurmeet Kaur *et al.*, 2018; Gurmeet Kaur and Mitchell, 2019).

Potassium feldspar

Representative compositions of Marepalli feldspar given in Table 4 confirm that they are essentially K-feldspar. There are no significant compositional differences between feldspars in leucite pseudomorphs and those occurring as poikilitic crystals in the groundmass. All are potassic (14.6–16.4 wt.% K_2O) with significant iron (0.3–1.4 wt.% Fe_2O_3), barium (<2 wt.% BaO) and very low sodium (<0.3 wt.% Na_2O) contents. The Marepalli K-feldspars are compositionally similar to those recorded in the Vattikod and Gundrapalli lamproites (Gurmeet Kaur *et al.*, 2018; Gurmeet Kaur and Mitchell, 2019). Additionally, the Vattikod lamproite also contains Na-feldspar (Gurmeet Kaur *et al.*, 2018). Feldspar with similar ferric content is also reported from worldwide lamproites (Mitchell and Bergman, 1991; Ngwenya and Tappe, 2021).

Spinels

Representative compositions of Marepalli spinels are given in Table 5. These are extremely rich in Cr_2O_3, but are unusually poor in TiO_2, and do not follow the trend T2 typical of lamproites (Fig. 9; Mitchell and Bergman, 1991). In zoned spinels, Cr_2O_3 and MgO contents decrease from core to rim accompanied by an increase in FeO_T and ZnO contents whereas Al_2O_3 and TiO_2 contents remain constant (Table 5). Groundmass spinels show compositional similarity to the rims of the zoned spinels (Fig. 9). The cores of zoned Marepalli spinels are enriched in Ti, Mg and Cr (3.9–5.2 wt.% TiO_2; 4.8–11.6 wt.% MgO; 53.6–56.3 wt.% Cr_2O_3), but poor in Al (1.9–2.8 wt.% Al_2O_3) and can be defined as titanian magnesian chromites (Fig. 9; Kumar *et al.*, 2021). Their FeO_T content ranges from 26.2–32.7 wt.%. The cores are marked by moderate Fe^{2+}_T# (0.56–0.79), low Ti# (0.06–0.08) with Fe^{3+}_T# (0.10–0.12), and therefore plot near the magnesiochromite–chromite edge on the Ti# *vs.* Fe^{2+}_T# compositional bivariate plot of the front face of the reduced iron spinel prism (Fig. 9). The rims of the zoned and the uniform groundmass Marepalli spinels are enriched in Ti (3.6–5.4 wt.% TiO_2) and Cr (47.1–52.0 wt.% Cr_2O_3), but poor in Al (1.3–2.5 wt.% Al_2O_3) and Mg (<3.3 wt.% MgO), so can be defined as titanian chromites (Fig. 9; Kumar *et al.*, 2021). Their FeO_T (31.9–36.3 wt.%) is relatively high and are characterised by high Fe^{2+}_T# (0.85 to 1), very low Ti# (0.06–0.09) and Fe^{3+}_T# (0.06–0.12), thus plot near the base and close to the chromite end of the magnesiochromite–chromite edge on the Ti# *vs.* Fe^{2+}_T# compositional bivariate plot of the front face of the reduced iron spinel prism (Fig. 9).

The compositions of the Marepalli spinels are characterised by an increase in Fe^{2+}_T# at nearly constant and low Ti# and do not

https://doi.org/10.1180/mgm.2022.49 Published online by Cambridge University Press

Table 2. Representative compositions (wt.%) of amphiboles (using the amphibole classification spreadsheet of Locock *et al*., 2014).

Main element oxides		1	2	3	4	5	6	7	8C	8R
Wt.%										
SiO_2		52.32	51.65	53.72	52.68	52.12	52.70	51.70	51.06	51.29
TiO_2		4.15	4.97	2.22	2.93	2.42	2.87	3.22	3.14	3.57
Al_2O_3		0.15	0.26	0.24	0.00	0.31	0.33	0.27	0.00	0.43
FeO*		16.34	17.67	14.22	18.52	16.50	16.87	18.99	23.28	17.69
MnO		0.23	0.23	0.33	0.32	0.28	0.29	0.30	0.45	0.29
MgO		12.14	10.93	14.02	10.50	12.08	11.97	10.37	7.17	10.77
CaO		3.68	3.15	4.04	3.02	4.11	4.13	3.98	4.06	4.18
Na_2O		4.82	5.00	4.88	4.97	4.41	4.60	4.57	4.66	4.66
K_2O		5.05	5.11	5.00	4.86	5.05	5.10	4.92	4.73	4.97
Total		98.88	98.97	98.67	97.80	97.28	98.86	98.32	98.55	97.85
FeO		16.34	17.67	13.81	18.52	16.50	16.87	18.99	23.28	17.69
Fe_2O_3		0.00	0.00	0.46	0.00	0.00	0.00	0.00	0.00	0.00
H_2O+		2.00	1.99	2.03	1.99	2.00	2.00	1.98	1.94	1.98
Structural formula calculated on the basis of 23 atoms of oxygen										
Formula assignments		K-KAT	Ti-K-KAT	K-RT	K-KAT	K-RT	K-RT	K-Fe^{2+}-RT	K-Fe^{2+}-RT	K-RT
T site	Si	7.766	7.715	7.885	7.954	7.867	7.838	7.815	7.868	7.762
	Al	0.026	0.046	0.042	–	0.055	0.058	0.048	–	0.077
	Ti	0.207	0.240	0.074	0.046	0.078	0.104	0.137	0.132	0.161
C site	Ti	0.256	0.319	0.172	0.287	0.197	0.217	0.230	0.232	0.246
	Al	–	–	–	–	–	–	–	–	–
	Fe3+	–	–	0.051	–	–	–	–	–	–
	Mn2+	0.029	0.029	0.015	0.012	0.002	0.030	0.033	0.059	0.037
	Fe2+	2.028	2.207	1.694	2.338	2.083	2.098	2.401	3.000	2.239
	Mg	2.686	2.434	3.068	2.363	2.718	2.654	2.337	1.647	2.430
B site	Mn2+	–	–	0.026	0.029	0.034	0.006	0.006	–	–
	Fe2+	–	–	–	–	–	–	–	–	–
	Ca	0.585	0.504	0.635	0.489	0.665	0.658	0.645	0.670	0.678
	Na	1.387	1.448	1.339	1.455	1.291	1.327	1.339	1.330	1.322
A site	Na	–	–	0.050	–	–	–	–	0.062	0.045
	K	0.956	0.974	0.936	0.936	0.972	0.968	0.949	0.930	0.960
OH		2.000	2.000	2.000	2.000	2.000	2.000	2.000	2.000	2.000
F		–	–	–	–	–	–	–	–	–

n.d. – not detected; FeO* – total Fe expressed as FeO; Fe_2O_3 and FeO calculated on a stoichiometric basis; C – Core; R – Rim.
Compositions: 1, 2, 8, included in titanite groundmass aggregates; 3–7, groundmass.
K-RT: potassic-richterite; K-Fe^{2+}-RT: potassic-ferro-richterite; K-KAT: potassic katophorite; Ti-K-KAT: Ti-rich potassic-katophorite; K-KAT: potassic katophorite.

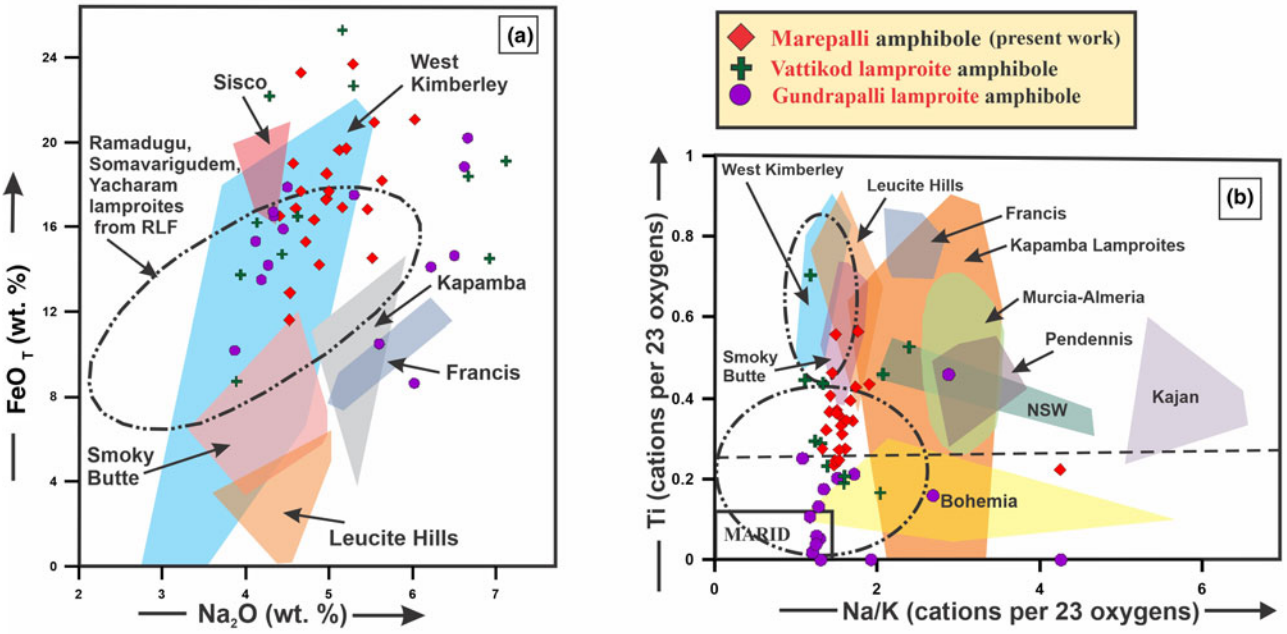

Fig. 7. (a) FeO_T (wt.%) *vs*. Na_2O (wt.%); and (b) Ti *vs*. Na/K (cations per 23 oxygens) compositional variation of amphiboles from Marepalli lamproite. Also shown is the field for amphibole from other Ramadugu lamproites (Chalapathi *et al.*, 2014) and the amphiboles from Vattikod and Gundrapalli lamproites (Gurmeet Kaur *et al.*, 2018; Gurmeet Kaur and Mitchell, 2019). The compositional field for amphibole in Kapamba lamproites is taken from Ngwenya and Tappe (2021). Compositional fields and trends for amphiboles in lamproites from Mitchell and Bergman (1991).

https://doi.org/10.1180/mgm.2022.49 Published online by Cambridge University Press

Table 3. Representative compositions (wt.%) of pyroxene.

Main element oxide	1	2	3	4	5	6	7	8#
Wt.%								
SiO_2	54.58	53.21	54.17	52.92	53.56	54.36	54.39	50.53
TiO_2	1.24	2.24	1.76	2.21	2.01	1.15	1.72	4.17
Al_2O_3	n.d.	0.33	0.29	0.34	0.35	0.24	0.29	0.68
Cr_2O_3	n.d.	0.58	0.72	0.98	0.91	0.81	0.99	0.52
FeO*	4.1	3.62	3.39	3.46	3.8	2.94	3.23	4.92
MnO	n.d.	n.d.	n.d.	n.d.	n.d.	n.d.	n.d.	0.05
MgO	17.09	17.3	17.37	17.52	17.05	17.71	17.44	14.85
CaO	23.41	23.19	23.26	23.43	22.7	23.31	23.18	22.53
Na_2O	0.3	0.39	n.d.	n.d.	0.46	n.d.	n.d.	0.57
Total	100.72	100.86	100.96	100.86	100.84	100.52	101.24	99.46
Recalculated analyses								
FeO	4.10	3.28	3.39	3.46	3.80	2.94	3.23	4.92
Fe_2O_3	–	0.37	–	–	–	–	–	–
Total	100.72	100.90	100.96	100.86	100.84	100.52	101.24	98.82
Structural formula calculated on the basis of 6 atoms of oxygen								
Si	1.817	1.771	1.803	1.761	1.783	1.809	1.810	1.682
Ti	0.031	0.056	0.044	0.055	0.050	0.029	0.043	0.104
Al	–	0.010	0.009	0.010	0.010	0.007	0.009	0.020
Cr	–	0.011	0.014	0.019	0.018	0.016	0.020	0.010
Fe^{2+}	0.057	0.046	0.047	0.048	0.053	0.041	0.045	0.068
Fe^{3+}	–	0.007	–	–	–	–	–	–
Mn	–	–	–	–	–	–	–	0.001
Mg	0.424	0.429	0.431	0.435	0.423	0.439	0.433	0.368
Ca	0.417	0.414	0.415	0.418	0.405	0.416	0.413	0.402
Na	0.005	0.006	–	–	0.007	–	–	0.009
End-member compositions (mol. %)								
Wo	0.46	0.47	0.46	0.46	0.46	0.46	0.46	0.48
En	0.47	0.48	0.48	0.48	0.48	0.49	0.49	0.44
Fs	0.06	0.05	0.05	0.05	0.06	0.05	0.05	0.08
Ca/(Ca+Mg)	0.50	0.49	0.49	0.49	0.49	0.49	0.49	0.52
Mg#	0.88	0.90	0.90	0.90	0.89	0.91	0.91	0.84

n.d. – not detected; FeO* – total Fe expressed as FeO; Fe^{2+} and Fe^{3+} calculated on a stoichiometric basis.
Compositions: 1–2, 6–7, microphenocrysts; 3–5, groundmass; 5–7, replaced by titanite along grain margin and cracks.
Composition 8# taken from Kumar *et al.* (2013).
Wo: Wollastonite ($CaSiO_3$); En: Enstatite ($MgSiO_3$); Fs: Ferrosilite ($FeSiO_3$).

follow any magmatic trend on the Ti# vs. Fe_T^{2+}# bivariate plot. These spinels are less evolved with compositional range from titanian magnesian chromite (TMC) to titanian chromite (TC), due to their low Ti and Fe^{3+} contents (Fig. 9). The Marepalli spinels are analogous to those in the Vattikod, Gundrapalli and Ramadugu cluster lamproites of Ramadugu Lamproite Field but exhibit a relatively wide range for Fe_T^{2+}# (Fig. 9; Chalapathi Rao *et al.*, 2014; Gurmeet Kaur *et al.*, 2018; Gurmeet Kaur and Mitchell, 2019). Marepalli spinels are characterised by the enrichment of Zn (up to 6.28 wt.% ZnO) and Mn (up to 3.6 wt.% MnO) trending from core towards rim (accompanied by groundmass grains), which are comparable to the spinels in the Vattikod lamproites (0.4–5.6 wt.% ZnO; 1.7–2.3 wt.% MnO; Gurmeet Kaur *et al.*, 2018) and Gundrapalli lamproite (up to 3.6 wt.% ZnO; up to 2.3 wt.% MnO; Gurmeet Kaur and Mitchell, 2019). However, the spinels occurring in the Ramadugu, Somavarigudem and Yacharam lamproites of Ramadugu Lamproite Field lack Zn but have high Mn content (0.95–1.4 wt.% MnO; Chalapathi Rao *et al.*, 2014).

Apatite

Representative compositions of Marepalli apatite are given in Table 6. These are enriched in SrO (up to 2.9 wt.%) and fluorine (up to 3.7 wt.%); a characteristic compositional feature found in lamproitic apatites (Mitchell and Bergman, 1991). These fluoroapatites are poor in FeO_T (<0.5 wt.%), MgO (<0.4 wt.%), Na_2O (<0.2 wt.%), K_2O (<0.2 wt.%) and lack BaO. The SiO_2 content varies from 0.5 to 1.9 wt.%. The rare earth element (REE) content is low (<0.8 wt.% Ce_2O_3; <0.6 wt.% Nd_2O_3). The Marepalli fluoroapatites are similar to those recorded previously from the Vattikod and the Gundrapalli lamproites (Gurmeet Kaur *et al.*, 2018; Gurmeet Kaur and Mitchell, 2019). The compositional zoning observed in one of the Marepalli apatite microphenocrysts indicates variation in its F, SrO and REE contents from core to rim. The core contains significant F (2.6 wt.%), low SrO (0.8 wt.%) and not detectable REE (by scanning electron microscopy), whereas the rim shows marked enrichment in F (3.5 wt.%) and SrO (2.9 wt.%) and has low REE (0.7 wt.% Ce_2O_3).

Titanite and allanite

Representative compositions of Marepalli titanite are given in Table 7. All textural varieties of titanite are compositionally similar and have low Al_2O_3 (1.2–2.3 wt.%), MgO (<0.9 wt.%) and FeO_T (1.4–1.7 wt.%). Similar titanite has also been reported previously from the Ramadugu, Somavarigudem, Yacharam, Vattikod and Gundrapalli lamproites (Chalapathi *et al.*, 2014; Gurmeet Kaur *et al.*, 2018; Gurmeet Kaur and Mitchell, 2019). Representative compositions of Marepalli allanite are given in Table 7. The Marepalli allanites are rich in FeO_T (14.4–15.0 wt.%) and CaO (11.4–12.4 wt.%) with significant amounts of Al_2O_3 (13.6–14.3 wt.%) and MgO (0.5–0.7 wt.%). These allanites are extremely enriched in LREEs (10.5–11.1 wt.% La_2O_3; 7.9–8.4 wt.% Ce_2O_3; 0.4–0.5 wt.% Nd_2O_3; 0.4–0.8 wt.% Pr_2O_3). Allanite is not a common phase in lamproites however it has been reported previously from the Vattikod lamproites (Gurmeet Kaur *et al.*, 2018).

Discussion and conclusions

Detailed mineralogical data for all primary major, minor and accessory phases are required for the correct characterisation and classification of lamproites and kimberlites (Scott Smith and Skinner, 1984; Mitchell and Bergman, 1991; Mitchell, 1995; Woolley *et al.*, 1996; Mitchell, 2020a). This investigation of the Marepalli dyke demonstrates that it is a *bona fide* lamproite. This conclusion is supported by the presence and distinct composition of the major typomorphic minerals of lamproite such as: Al-poor, Ti-Fe-rich phlogopite; pseudoleucite; Ti-K-rich richterite; Al-Na-poor diopside; Al-poor titanian magnesian chromite and titanian chromite. Minor and accessory minerals are Sr-F-rich, REE-poor apatite together with late-stage residual titanite and K-feldspar. The alumina-poor phlogopites display compositional zonation trends of almost constant Al_2O_3 with increasing FeO_T and TiO_2 as compared to the archetypal kimberlites and typically occupy the lamproite fields (Fig. 6a–b). The alumina-poor (Al_2O_3 <0.7 wt.%) amphiboles exhibit compositional evolution from titanian potassic-katophorite through potassic-ferro-katophorite, potassic-katophorite, potassic-ferro-richterite, potassic-richterite to titanian potassic-arfvedsonite, and show affinity with those in the West Kimberley (Fig. 7a), Smoky Butte and Leucite Hills lamproites (Fig. 7b). All the pyroxenes are diopsidic in composition with low Al_2O_3 (<0.4 wt.%), Na_2O (<0.6 wt.%), and fall well within the lamproite field (Fig. 8). The spinels are alumina-poor (Al_2O_3 <2.8 wt.%), with compositional evolution from titanian magnesian chromite (TMC) cores to titanian

https://doi.org/10.1180/mgm.2022.49 Published online by Cambridge University Press

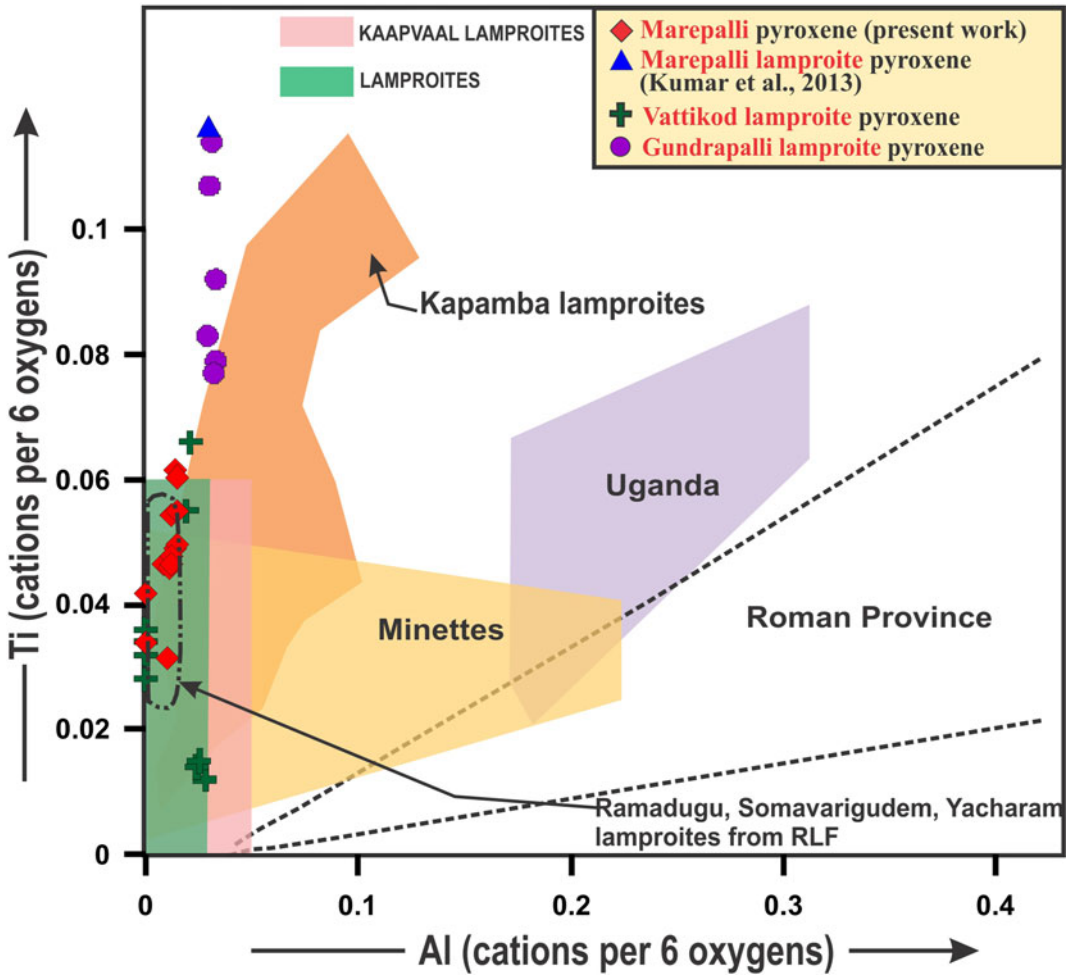

Fig. 8. Compositional variation (Ti *vs*. Al in atoms per formula unit) of pyroxenes from Marepalli lamproite. Also shown are the pyroxenes from Vattikod and Gundrapalli lamproites (Gurmeet Kaur *et al.*, 2018; Gurmeet Kaur and Mitchell, 2019). Compositional fields and trends for lamproites, minettes, Roman province lavas and kamafugites from Mitchell and Bergman (1991). The dotted circular field for spinels from other Ramadugu lamproites is shown (Chalapathi *et al.*, 2014). The compositional field for pyroxene in Kapamba lamproites is taken from Ngwenya and Tappe (2021). RLF – Ramadugu lamproite field.

Table 4. Representative compositions (wt.%) of K-feldspar.

Main element oxides	1	2	3	4	5	6	7	8	9	10	11#
Wt.%											
SiO_2	65.29	64.36	64.68	64.58	65.00	65.13	64.74	64.76	65.62	66.06	65.60
TiO_2	n.d.	n.d.	n.d.	n.d.	n.d.	n.d.	n.d.	n.d.	n.d.	n.d.	0.01
Al_2O_3	17.70	17.82	17.33	16.75	16.53	18.27	18.74	18.16	18.01	17.74	17.79
Cr_2O_3	n.d.	n.d.	n.d.	n.d.	n.d.	n.d.	n.d.	n.d.	n.d.	n.d.	0.03
Fe_2O_3	1.12	1.35	0.99	0.83	0.53	0.51	0.45	0.55	0.61	0.82	0.18
MgO	n.d.	n.d.	n.d.	n.d.	n.d.	n.d.	n.d.	n.d.	n.d.	n.d.	0.05
CaO	n.d.	n.d.	n.d.	2.16	1.54	n.d.	n.d.	n.d.	n.d.	n.d.	n.d.
Na_2O	0.25	0.29	0.27	0.28	0.26	0.19	0.25	n.d.	n.d.	n.d.	0.12
K_2O	15.59	15.67	15.94	14.58	14.92	16.36	16.05	16.26	16.08	16.31	16.13
BaO	0.30	0.33	n.d.	1.45	1.22	n.d.	0.44	n.d.	n.d.	n.d.	n.d.
Total	100.25	99.82	99.21	100.63	100.00	100.46	100.67	99.73	100.32	100.93	99.91
Structural formula calculated on the basis of 8 atoms of oxygen											
Si	2.943	2.991	3.016	3.001	3.028	2.999	2.980	3.001	3.017	3.023	3.027
Ti	–	–	–	–	–	–	–	–	–	–	–
Al	1.049	0.976	0.953	0.917	0.908	0.991	1.017	0.992	0.976	0.957	0.967
Cr	–	–	–	–	–	–	–	–	–	–	0.001
Fe^{3+}	0.039	0.047	0.035	0.029	0.019	0.018	0.016	0.019	0.021	0.028	0.006
Mg	–	–	–	–	–	–	–	–	–	–	0.003
Ca	–	–	–	0.108	0.077	–	–	–	–	–	–
Na	0.023	0.026	0.024	0.025	0.023	0.017	0.022	–	–	–	0.011
K	0.930	0.929	0.948	0.864	0.887	0.961	0.943	0.961	0.943	0.952	0.949
Ba	0.005	0.006	–	0.026	0.022	–	0.008	–	–	–	–
Calculated parameters											
K/(K+Na+Ca)	0.98	0.97	0.97	0.87	0.90	0.98	0.98	1.00	1.00	1.00	0.99
Na/(Na+Ca+K)	0.02	0.03	0.03	0.03	0.02	0.02	0.02	–	–	–	0.01
Ca/(Ca+Na+K)	–	–	–	0.11	0.08	–	–	–	–	–	–

n.d. – not detected; total iron expressed as Fe_2O_3
Compositions: 1–5, 9–10, groundmass (mesostasis); 6–8, present in leucite pseudomorphs; 11# taken from Kumar *et al.*, 2013.

https://doi.org/10.1180/mgm.2022.49 Published online by Cambridge University Press

Table 5. Representative compositions (wt.%) of spinels.

Main element oxides	1	2	3	4	5	6	7	8	9C	9R	10C	10R	11C	11R	12	13	14	15	16C	16R
Wt.%																				
SiO_2	0.59	0.79	0.8	0.71	0.84	0.55	0.51	0.73	n.d.	n.d.	n.d.	n.d.	n.d.	n.d.	0.42	0.32	0.32	0.43	0.33	0.39
TiO_2	3.9	5.42	3.61	3.59	3.62	3.94	4.95	3.8	4.13	4.05	3.89	3.87	3.99	3.9	4.89	4.63	4.54	4.36	5.22	4.53
Al_2O_3	2.44	1.34	2.16	2.19	2.15	2.51	2.04	2.28	2.76	2.5	2.75	2.14	2.71	2.43	1.79	2.06	2.05	2.23	1.99	1.94
Cr_2O_3	50.89	47.13	49.49	50.09	49.02	51.29	49.24	50.31	54.79	52.01	53.6	50.54	56.29	51.36	51.09	52.86	51.01	48.48	54.97	51.44
FeO*	33.47	33.43	32.5	31.9	32.07	33.06	33.14	32.51	28.00	33.81	32.7	33.71	26.23	34.38	36.1	31.45	36.32	35.14	26.32	33.06
MnO	3.28	3.63	3.13	3.05	3.13	3.37	3.42	3.13	1.22	2.66	2.41	2.82	0.91	2.9	2.04	1.3	1.9	2.12	n.d.	1.64
MgO	n.d.	n.d.	n.d.	n.d.	n.d.	1.34	0.32	0.27	9.46	2.00	4.8	1.16	10.88	1.91	0.69	6.6	2.45	0.8	11.62	3.3
ZnO	2.89	5.79	5.94	6.24	6.28	2.83	5.67	5.98	n.d.	3.29	0.42	4.78	n.d.	3.25	3.07	n.d.	0.83	4.46	n.d.	2.93
Total	97.46	97.53	97.63	97.77	97.11	98.29	99.78	99.01	100.36	100.32	100.57	99.02	101.01	100.13	100.09	99.22	99.42	98.02	100.45	99.23
Recalculated analyses																				
Fe_2O_3	3.81	5.45	5.62	5.28	5.61	5.14	4.04	5.53	8.02	6.92	7.26	7.77	8.04	7.84	5.11	6.67	6.56	6.88	7.01	6.24
FeO	30.04	28.53	27.44	27.15	27.02	28.43	29.50	27.53	20.78	27.58	26.17	26.71	19.00	27.32	31.50	25.45	30.42	28.95	20.01	27.44
Structural formula calculated on the basis of 3 cations																				
Si	0.022	0.030	0.030	0.027	0.032	0.020	0.019	0.027	–	–	–	–	–	–	0.015	0.011	0.012	0.016	0.011	0.014
Ti	0.111	0.155	0.103	0.102	0.103	0.109	0.137	0.106	0.106	0.110	0.103	0.108	0.100	0.106	0.135	0.123	0.124	0.122	0.132	0.123
Al	0.108	0.060	0.096	0.097	0.096	0.109	0.089	0.100	0.111	0.106	0.114	0.093	0.107	0.104	0.077	0.085	0.088	0.098	0.079	0.083
Cr	1.518	1.415	1.478	1.495	1.472	1.491	1.435	1.479	1.473	1.485	1.489	1.476	1.490	1.470	1.481	1.470	1.462	1.431	1.458	1.472
Fe^{3+}	0.108	0.156	0.160	0.150	0.160	0.142	0.112	0.155	0.205	0.188	0.192	0.216	0.202	0.214	0.141	0.177	0.179	0.193	0.177	0.170
Fe^{2+}	0.948	0.906	0.867	0.857	0.859	0.874	0.910	0.856	0.591	0.833	0.769	0.825	0.532	0.827	0.966	0.749	0.922	0.904	0.562	0.831
Mn	0.105	0.117	0.100	0.098	0.101	0.105	0.107	0.099	0.035	0.081	0.072	0.088	0.026	0.089	0.063	0.039	0.058	0.067	–	0.050
Mg	–	–	–	–	–	0.073	0.018	0.015	0.480	0.108	0.251	0.064	0.543	0.103	0.038	0.346	0.132	0.045	0.581	0.178
Zn	0.080	0.162	0.166	0.174	0.176	0.077	0.154	0.164	–	0.088	0.011	0.130	–	0.087	0.083	–	0.022	0.123	–	0.078
Calculated parameters																				
$Fe^{2+*}/(Fe^{2+*}+Mg)$	1.00	1.00	1.00	1.00	1.00	0.93	0.98	0.99	0.62	0.90	0.79	0.94	0.57	0.91	0.97	0.73	0.89	0.96	0.56	0.85
$Fe^{2+}/(Fe^{2+}+Mg)$	1.00	1.00	1.00	1.00	1.00	0.92	0.98	0.98	0.55	0.88	0.75	0.93	0.49	0.89	0.96	0.68	0.87	0.95	0.49	0.82
Cr/(Cr+Al)	0.93	0.96	0.94	0.94	0.94	0.93	0.94	0.94	0.93	0.93	0.93	0.94	0.93	0.94	0.95	0.94	0.94	0.93	0.95	0.95
Ti/(Ti+Al+Cr)	0.06	0.09	0.06	0.06	0.06	0.06	0.08	0.07	0.07	0.06	0.06	0.07	0.06	0.07	0.08	0.07	0.07	0.07	0.08	0.07
$Fe^{3+}/(Fe^{3+}+Al+Cr)$	0.06	0.10	0.09	0.09	0.09	0.08	0.07	0.09	0.11	0.11	0.11	0.12	0.11	0.12	0.08	0.10	0.10	0.11	0.10	0.10

n.d. – not detected; FeO* – total Fe expressed as FeO; Fe_2O_3 and FeO calculated on a stoichiometric basis; C – Core and R – Rim.
Compositions: 1–8, 12–15, groundmass; 9–11, 16, included in olivine pseudomorphs at rims.

Table 5. Representative compositions (wt.%) of spinels (continued).

Main element oxides	17C#	17R#	18#	19#	20#	21#	22#	23C#	23R#
Wt.%									
SiO_2	0.33	0.39	0.32	0.32	n.d.	0.42	n.d.	n.d.	n.d.
TiO_2	5.22	4.53	4.63	4.54	5.08	4.89	4.32	4.81	4.67
Al_2O_3	1.99	1.94	2.06	2.05	1.89	1.79	1.75	2.08	1.81
Cr_2O_3	54.97	51.44	52.86	51.01	46.97	51.09	49.79	54.74	51.21
FeO*	26.32	33.06	31.45	36.32	38.41	36.1	34.21	27.1	34.21
MnO	n.d.	1.64	1.30	1.90	2.3	2.04	2.15	n.d.	1.85
MgO	11.62	3.30	6.60	2.45	6.87	0.69	0.96	10.59	2.13
ZnO	n.d.	2.93	n.d.	0.83	3.28	3.07	3.64	n.d.	3.17
Total	100.45	99.23	99.22	99.42	104.8	100.09	96.82	99.32	99.05
Recalculated analyses									
Fe_2O_3	7.01	6.24	6.67	6.56	17.19	5.11	6.50	7.40	6.52
FeO	20.01	27.44	25.45	30.42	22.94	31.50	28.36	20.44	28.35
Structural formula calculated on the basis of 3cations									
Si	0.011	0.014	0.011	0.012	–	0.015	–	–	–
Ti	0.132	0.123	0.123	0.124	0.128	0.135	0.123	0.124	0.129
Al	0.079	0.083	0.085	0.088	0.074	0.077	0.078	0.084	0.078
Cr	1.458	1.472	1.470	1.462	1.239	1.481	1.491	1.479	1.484
Fe^{3+}	0.177	0.170	0.177	0.179	0.432	0.141	0.185	0.190	0.180
Fe^{2+}	0.562	0.831	0.749	0.922	0.640	0.966	0.898	0.584	0.869
Mn	–	0.050	0.039	0.058	0.065	0.063	0.069	–	0.057
Mg	0.581	0.178	0.346	0.132	0.342	0.038	0.054	0.539	0.116
Zn	–	0.078	–	0.022	0.081	0.083	0.102	–	0.086
Calculated parameters									
$Fe^{2+*}/(Fe^{2+*}+Mg)$	0.57	0.85	0.73	0.89	0.77	0.97	0.95	0.60	0.90
$Fe^{2+}/(Fe^{2+}+Mg)$	0.49	0.82	0.68	0.87	0.65	0.96	0.94	0.52	0.88
Cr/(Cr+Al)	0.95	0.95	0.95	0.94	0.94	0.95	0.95	0.95	0.95
Ti/(Ti+Al+Cr)	0.08	0.07	0.07	0.07	0.09	0.08	0.07	0.07	0.08
$Fe^{3+}/(Fe^{3+}+Al+Cr)$	0.10	0.10	0.10	0.10	0.25	0.08	0.11	0.11	0.10

n.d. – not detected; FeO* – total Fe expressed as FeO; C – Core and R – Rim; Fe_2O_3 and FeO calculated on a stoichiometric basis.
Compositions: 17# – 23#, Gundrapalli spinels.

https://doi.org/10.1180/mgm.2022.49 Published online by Cambridge University Press

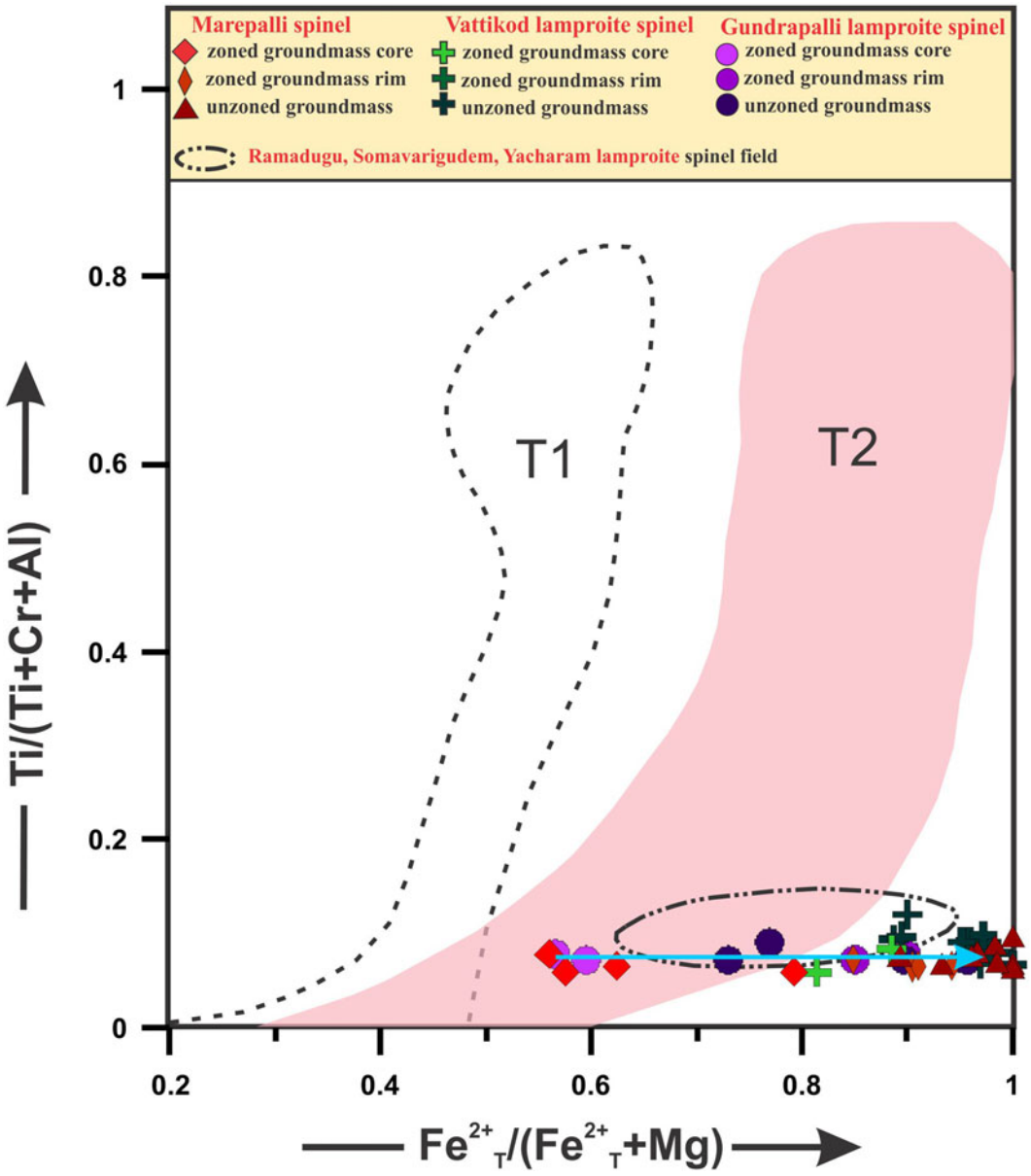

Fig. 9. Compositional variation of spinels from Marepalli and Gundrapalli lamproite projected onto the front face of the reduced iron-spinel compositional prism (Mitchell, 1986). Compositional fields and trends for spinels from kimberlites (T1) and lamproites (T2) from Mitchell (1986, 1995). The dotted circular field for spinels from other Ramadugu lamproites is shown (Chalapathi *et al.*, 2014). Also shown are the spinels from Vattikod lamproite (Gurmeet Kaur *et al.*, 2018). The blue arrow shows the compositional evolutionary trend of spinels from core to rim.

chromite (TC) rims and groundmass grains, marked by an increase in Fe^{2+}_{T}# at nearly constant and low Ti# and Fe^{3+}# (Fig. 9). The fluoroapatites are characterised by low Sr content in the cores and Sr and F enrichment in the rims, again typical of lamproites. Former euhedral olivine and anhedral leucite are now present as pseudomorphs in the Marepalli rock. The rock might have undergone late-stage/post-magmatic carbonisation and silicification which led to the secondary replacement of leucite grains by calcite and quartz.

According to the above mineralogical data using a mineralogical genetic classification scheme for potassic-ultrapotassic rocks, we classify the Marepalli dyke rock as a 'pseudoleucite-amphibole-phlogopite lamproite'. Although typomorphic minerals such as the priderite group and wadeite are absent in the Marepalli rock, the presence of abundant Ti-rich, Al-poor phlogopite, primary clinopyroxene (diopside), K-richterite, K-feldspar, leucite (now pseudomorphed) and titanite clearly support a lamproite classification. The absence of monticellite, abundant primary carbonates (calcite and/or dolomite) and melilite clearly exempt the Marepalli rock from being classified as kimberlite or an ultramafic lamprophyre (Mitchell and Bergman, 1991; Mitchell, 1986, 1995; Tappe *et al.*, 2005; Mitchell, 2020a).

The increasing FeO_T content accompanied by significant MgO depletion at almost constant Al_2O_3 in Marepalli phlogopite rims and groundmass indicate the $^{VI}Fe^{2+}$ enrichment and highlight the reducing state of the evolving magma (Mitchell and Bergman, 1991). Similarly, low FeO_T in clinopyroxene (diopside) and absence of aegirine also support the low oxidation state of the evolving magma. The crystallisation of F-bearing phlogopite and F-rich apatite also indicate the reducing environment

https://doi.org/10.1180/mgm.2022.49 Published online by Cambridge University Press

Table 6. Representative compositions (wt.%) of apatite.

Main element oxides	1	2	3	4	5	6C	6R	7
Wt.%								
SiO_2	1.93	0.95	1.05	1.3	0.91	0.48	1.13	1.52
FeO*	0.54	0.24	n.d.	0.31	0.26	0.25	n.d.	n.d.
MgO	0.41	0.31	0.19	0.32	n.d.	n.d.	n.d.	0.33
CaO	52.22	52.21	51.42	52.19	51.9	52.82	51.78	51.4
SrO	2.67	2.38	2.86	2.41	2.55	0.8	2.59	2.52
Na_2O	n.d.	n.d.	0.24	n.d.	n.d.	1.2	n.d.	n.d.
K_2O	n.d.	0.13	0.17	n.d.	n.d.	n.d.	n.d.	n.d.
P_2O_5	39.46	40.72	40.3	40.03	44.42	44.13	44.97	39.54
Ce_2O_3	0.72	n.d.	0.63	0.74	n.d.	n.d.	0.79	0.82
Nd_2O_3	0.41	0.57	n.d.	n.d.	n.d.	n.d.	n.d.	0.37
F	2.86	3.38	2.9	3.3	3.48	2.85	3.52	3.1
Total	98.36	97.51	96.86	97.3	100.04	99.68	101.26	96.5

n.d. – not detected; FeO*total Fe expressed as FeO; C – Core and R – Rim.
Compositions: 1, apatite included in phlogopite; 2–3, groundmass apatites; 4–5, phenocrystal apatites; 6–7, apatites partially included in pyroxenes.

conditions (Foley *et al.*, 1986; Talukdar *et al.*, 2018). The low Ti# and Fe^{3+}# of Marepalli spinels could be due to their crystallisation from less evolved magma composition or crystallisation from magma under reducing conditions (Mitchell, 1986). The Marepalli spinels show a narrow compositional range from titanian magnesian chromite to titanian chromite and are similar to those in Hills Pond lamproite (Mitchell, 1985), TK4 lamproite of the Wajrakarur Lamproite Field (Shaikh *et al.*, 2017) and the Aliyabad lamproite of the Banganapalle Lamproite Field (Kumar *et al.*, 2021). These zoned spinels are exceptionally enriched in Mn and Zn which might be due to the high oxygen fugacity of the magma or enrichment by the hydrothermal process as suggested by Kumar *et al.* (2021). However the particular compositions of phlogopite, clinopyroxene, apatite and spinels clearly rule out an increase in the oxidation state of the magma during evolution. Thus, the Mn–Zn enrichment in rims of Marepalli spinels could be due to the hydrothermal processes as inferred for Aliyabad spinels (Kumar *et al.*, 2021). Mn and Zn enrichment in spinel rims occur by the substitution of Mg^{2+} and Fe^{2+} by Mn and Zn when the magma interacts with mineralising fluids enriched in Mn and Zn (Fanlo *et al.*, 2015).

Table 7. Representative compositions (wt.%) of titanite and allanite.

Main element oxides	titanite 1	2	3	4	5	allanite 6	7	8
Wt.%								
SiO_2	31.53	32.71	31.8	31.53	32.4	37.97	33.29	33.91
TiO_2	36.4	35.02	35.68	36.81	32.13	n.d.	n.d.	n.d.
Al_2O_3	1.5	1.77	1.89	1.52	2.11	13.58	14.28	14.29
FeO*	1.41	1.59	1.73	1.66	1.71	14.43	14.96	15.01
MgO	0.41	0.87	0.47	0.37	0.96	0.65	0.54	0.55
CaO	27.37	26.98	26.84	26.87	27.15	11.36	12.41	12.41
Na_2O	0.14	0.14	0.11	n.d.	n.d.	n.d.	n.d.	n.d.
K_2O	n.d.	0.24	0.14	n.d.	n.d.	n.d.	n.d.	n.d.
La_2O_3	n.d.	n.d.	n.d.	n.d.	n.d.	11.06	11.14	10.48
Ce_2O_3	n.d.	n.d.	n.d.	n.d.	n.d.	7.93	8.39	8
Pr_2O_3	n.d.	n.d.	n.d.	n.d.	n.d.	0.81	0.57	0.37
Nd_2O_3	n.d.	n.d.	n.d.	n.d.	n.d.	0.38	0.47	0.35
Total	98.76	99.32	98.66	98.76	96.63	98.17	96.05	95.37
Structural formula calculated on the basis of 4 atoms of oxygen						Structural formula calculated on the basis of 8 cations		
Si	0.831	0.855	0.838	0.831	0.871	3.557	3.207	3.26
Ti	0.722	0.688	0.707	0.729	0.649	–	–	–
Al	0.047	0.055	0.059	0.047	0.067	1.5	1.621	1.619
Fe^{2+*}	0.031	0.035	0.038	0.037	0.038	1.017	1.085	1.086
Mg	0.016	0.034	0.018	0.015	0.038	0.091	0.078	0.079
Ca	0.773	0.756	0.758	0.758	0.782	1.14	1.281	1.278
Na	0.007	0.007	0.006	–	–	–	–	–
K	–	0.008	0.005	–	–	–	–	–
La	–	–	–	–	–	0.382	0.396	0.372
Ce	–	–	–	–	–	0.272	0.296	0.282
Pr	–	–	–	–	–	0.028	0.02	0.013
Nd	–	–	–	–	–	0.013	0.016	0.012

n.d. – not detected; FeO* – total Fe expressed as FeO
Compositions: 1–4, groundmass titanite aggregates enclosing amphiboles; 5, titanite along margin of olivine pseudomorph; 6–8, allanite included in leucite pseudomorph.

The Marepalli dyke represents a particular variety of lamproite crystallised from Na-Ca-Al poor and Ti-Cr-K rich magma derived from the partial melting of a local metasomatised mantle source. It can be related genetically to the Vattikod, Gundrapalli and Ramadugu cluster, which lies in close proximity, in the Ramadugu Lamproite Field. The minor mineralogical variations in the intra-field lamproites are a result of the differentiation of the common parent magma (Gurmeet Kaur *et al.*, 2018).

Acknowledgements. GK is grateful to Panjab University for granting her leave to carry out studies on Marepalli lamproite at Lakehead University, Thunder Bay, Ontario. The authors wish to acknowledge Dr. Somnath Thakur for helping us in the geo-referencing of the map. JS and PK, senior research fellows at Panjab University, Chandigarh are thankful to CSIR for awarding them the fellowship. The authors are thankful to Prof. Sebastian Tappe and an anonymous reviewer for the critical review and their valuable comments and suggestions that helped to improve the manuscript.

Competing interests. The authors declare none

References

Ahmed S., Sufija M.V. and Ravi S. (2016) *Final report on search for kimberlite/lamproite in Kollapur–Srirangapur blocks in parts of Mahabubnagar district, Telangana and Kurnool district, Andhra Pradesh* (*G-4 stage*). Unpublished progress report of the Geological Survey of India for field seasons 2014–15 and 2015–16.

Chakrabarti R., Basu A.R. and Paul D.K. (2007) Nd-Hf-Sr-Pb isotopes and trace element geochemistry of Proterozoic lamproites from southern India: Subducted komatiite in the source. *Chemical Geology*, **236**, 291–302.

Chalapathi Rao N.V., Kamde G., Kale H.S. and Dongre A. (2010) Petrogenesis of the Mesoproterozoic lamproites from the Krishna valley, eastern Dharwar craton, southern India. *Precambrian Research* **177**, 103–130.

Chalapathi Rao N.V., Kumar A., Sahoo S., Dongre A.N. and Talukdar D. (2014) Petrology and petrogenesis of Mesoproterozoic lamproites from the Ramadugu field, NW margin of the Cuddapah basin, Eastern Dharwar craton, southern India. *Lithos*, **196**, 150–168.

Chalapathi Rao N.V., Giri R.K., Sharma A. and Pandey A. (2020) Lamprophyres from the Indian shield: A review of their occurrence, petrology, tectonomagmatic significance and relationship with the Kimberlites and related rocks. *Episodes Journal of International Geoscience*, **43**, 231–248.

Dongre A. and Tappe S. (2019) Kimberlite and carbonatite dykes within the Premier diatreme root (Cullinan Diamond Mine, South Africa): New insights to mineralogical-genetic classifications and magma CO_2 degassing. *Lithos*, **338**, 155–173.

Fanlo I., Gervilla F., Colás V. and Subías I. (2015) Zn-, Mn-and Co-rich chromian spinels from the Bou-Azzer mining district (Morocco): constraints on their relationship with the mineralizing process. *Ore Geology Reviews*, **71**, 82–98.

Fareeduddin and Mitchell R.H. (2012) *Diamonds and their Source Rocks in India*. Geological Society of India, Bangalore, India, 434pp.

Foley S.F., Taylor W.R. and Green D.H. (1986) The role of fluorine and oxygen fugacity in the genesis of the ultrapotassic rocks. *Contributions to Mineralogy and Petrology*, **94**, 382–392.

Gurmeet Kaur and Mitchell R.H. (2013) Mineralogy of P2-West 'Kimberlite', Wajrakarur Kimberlite Field, Andhra Pradesh, India: kimberlite or lamproite? *Mineralogical Magazine*, **77**, 3175–3196.

Gurmeet Kaur and Mitchell R.H. (2016) Mineralogy of the P-12 K-Ti-richterite diopside olivine lamproite from Wajrakarur, Andhra Pradesh, India: implications for subduction-related magmatism in eastern India. *Mineralogy and Petrology*, **110**, 223–245.

Gurmeet Kaur and Mitchell R.H. (2019) Mineralogy of the baotite-bearing Gundrapalli lamproite, Nalgonda district, Telangana, India. *Mineralogical Magazine*, **83**, 401–411.

Gurmeet Kaur, Korakoppa M., Fareeduddin and Pruseth K.L. (2013) Petrology of P-5 and P-13 "kimberlites" from Lattavaram kimberlite cluster, Wajrakarur Kimberlite Field, Andhra Pradesh, India: reclassification as lamproites. Pp 183–194 in: *Proceedings of the Xth International Kimberlite Conference* (D.G. Pearson, H.S. Grutter, J.W. Harris, B.A. Kjarsgaard, H. O'brien, N.V Chalapathi Rao and R.S.J. Sparks, editors). Geological Society of India, Springer Publication.

Gurmeet Kaur, Mitchell R.H. and Ahmed S. (2018) Mineralogy of the Vattikod lamproite dykes, Ramadugu lamproite field, Nalgonda District, Telangana: A possible expression of ancient subduction-related alkaline magmatism along Eastern Ghats Mobile Belt, India. *Mineralogical Magazine*, **82**, 35–58.

Jayananda M., Santosh M. and Aadhiseshan K.R. (2018) Formation of Archean (3600–2500 Ma) continental crust in the Dharwar Craton, southern India. *Earth-Science Reviews*, **181**, 12–42.

Krmíček L., Magna T., Pandey A., Rao N.C. and Kynický J. (2022) Lithium isotopes in kimberlites, lamproites and lamprophyres as tracers of source components and processes related to supercontinent cycles. *Geological Society, London, Special Publications*, **513**, 209–236.

Kumar A., Ahmed S., Priya R. and Sridhar M. (2013) Discovery of lamproites near Vattikod area, NW margin of the Cuddapah basin, Eastern Dharwar craton, southern India. *Journal of the Geological Society of India*, **82**, 307–312.

Kumar A., Parashuramulu V. and Nagaraju E. (2015) A 2082 Ma radiating dyke swarm in the Eastern Dharwar Craton, southern India and its implications to Cuddapah basin formation. *Precambrian Research*, **266**, 490–505.

Kumar S.P., Shaikh A.M., Patel S.C., Sheikh J.M., Behera D., Pruseth K.L., Ravi S. and Tappe S. (2021) Multi-stage magmatic history of olivine–leucite lamproite dykes from Banganapalle, Dharwar craton, India: evidence from compositional zoning of spinel. *Mineralogy and Petrology*, **115**, 87–112.

Liferovich R.P. and Mitchell R.H. (2005) Composition and paragenesis of Na-, Nb-, and Zr-bearing titanite from Khibina, Russia, and crystal structure data for synthetic analogues. *The Canadian Mineralogist*, **43**, 795–812.

Locock A.J. (2014) An Excel spreadsheet to classify chemical analyses of amphiboles following the IMA 2012 recommendations. *Computers & Geosciences*, **62**, 1–11.

Mitchell R.H. (1985) A review of the mineralogy of lamproites. *Transactions of the Geological Society of South Africa*, **88**, 411–437.

Mitchell R.H. (1986) *Kimberlites: Mineralogy, Geochemistry and Petrology*. Plenum Press, New York, 978pp.

Mitchell R.H. (1994) The lamprophyre facies. *Mineralogy and Petrology*, **51**(2–4), 137–146.

Mitchell R.H. (1995) *Kimberlites, Orangeites, and Related Rocks*. Plenum Press, New York, 410pp.

Mitchell R.H. (2020a) Potassic alkaline rocks: leucitites, lamproites, and kimberlites. In: *Reference Module in Earth Systems and Environmental Sciences*, 1–25, doi: 10.1016/B978-0-12-409548-9.12482-0

Mitchell R.H. (2020b) Igneous rock associations 26. Lamproites, exotic potassic alkaline rocks: a review of their nomenclature, characterization and origins. *Geoscience Canada: Journal of the Geological Association of Canada/ Geoscience Canada: journal de l'Association Géologique du Canada*, **47**, 119–142.

Mitchell R.H. and Bergman S.C. (1991) *Petrology of Lamproites*. Plenum Press, New York, 447pp.

Murphy D.T., Collerson K.D. and Kamber B.S. (2002) Lamproites from Gaussberg, Antarctica: possible transition zone melts of Archaean subducted sediments. *Journal of Petrology*, **43**, 981–1001.

Naqvi S.M. and Rogers J.J.W. (1987) *Precambrian Geology of India*. Oxford monographs on Geology and Geophysics No. 6. Oxford University Press, Oxford, UK, 223pp.

Ngwenya N.S. and Tappe S. (2021) Diamondiferous lamproites of the Luangwa Rift in central Africa and links to remobilized cratonic lithosphere. *Chemical Geology*, **568**, 120019.

Pandey A. and Chalapathi Rao N.V. (2020) Supercontinent transition as a trigger for ~1.1 Gyr diamondiferous kimberlites and related magmatism in India. *Lithos*, **370–371**, 105620, https://doi.org/10.1016/j.lithos.2020.105620

Prelević D., Foley S.F., Romer R. and Conticelli S. (2008) Mediterranean Tertiary lamproites derived from multiple source components in postcollisional geodynamics. *Geochimica et Cosmochimica Acta*, **72**, 2125–2156.

Ramakrishnan M. and Vaidyanadhan R. (2008) *Geology of India, vol. I & II*. Geological Society of India, Bangalore.

Ravi S., Sufija M.V., Patel S.C., Sheikh J.M., Sridhar M., Kaminsky F.V., Khachatryan G.K., Nayak S.S. and Bhaskara Rao K.S. (2013) Diamond potential of the Eastern Dharwar Craton, southern India, and a reconnaissance study of physical and infrared characteristics of the diamonds. Pp. 335–348 in: *Proceedings of 10th International Kimberlite Conference*. Springer, New Delhi.

Rieder M., Cavazzini D., Yakonov Y.S.D., Frank-Kamenetskii V.A., Gottardi G., Guggenheim S., Koval P.V., Muller G., Neiva A.M.R., Radoslovich E.W., Robert J.L., Sassi F.P., Takeda H., Weiss Z. and Wones D.R. (1998) Nomenclature of the micas. *The Canadian Mineralogist*, **36**, 905–912.

Scott Smith B.H. and Skinner E.M.W. (1984) Diamondiferous lamproites. *Journal of Geology*, **92**, 433–438.

Scott Smith B.H., Nowicki T.E., Russell J.K., Webb K.J., Mitchell R.H., Hetman C.M. and Robey J.V. (2018) *A Glossary of Kimberlite and Related Terms Part 1: Glossary*. Scott-Smith Petrology Inc., North Vancouver, British Columbia, Canada, 144 pp.

Shaikh A.M., Patel S.C., Ravi S., Behera D. and Pruseth K.L. (2017) Mineralogy of the TK1 and TK4 'kimberlites' in the Timmasamudram cluster, Wajrakarur kimberlite field, India: Implications for lamproite magmatism in a field of kimberlites and ultramafic lamprophyres. *Chemical Geology*, **455**, 208–230.

Shaikh A.M., Kumar S.P., Patel S.C., Thakur S.S., Ravi S. and Behera D. (2018) The P3 kimberlite and P4 lamproite, Wajrakarur kimberlite field, India: mineralogy, and major and minor element compositions of olivines as records of their phenocrystic vs xenocrystic origin. *Mineralogy and Petrology*, **112**, 609–624.

Shaikh A.M., Patel S.C., Bussweiler Y., Kumar S.P., Tappe S., Ravi S. and Mainkar D. (2019) Olivine trace element compositions in diamondiferous lamproites from India: Proxies for magma origins and the nature of the lithospheric mantle beneath the Bastar and Dharwar cratons. *Lithos*, **324**, 501–518.

Sridhar M. and Rau T.K. (2005) Discovery of a new lamproite field—Ramadugu lamproite field (RLF), Nalgonda District, Andhra Pradesh. Pp. 55–57 in: *Proceedings of the Group Discussion on Kimberlites and Related Rocks of India*. Organized by the Geological Society of India, Bangalore, India [Extended abstracts].

Srivastava R.K., Samal A.K. and Gautam G.C. (2015) Geochemical characteristics and petrogenesis of four Palaeoproterozoic mafic dike swarms and associated large igneous provinces from the eastern Dharwar craton, India. *International Geology Review*, **57**(11–12), 1462–1484.

Swaminath J. and Ramakrishnan M. (1981) Early Precambrian Supracrustals of Southern Karnataka. *Memoirs of Geological Survey of India*, **112**, 350.

Talukdar D., Pandey A., Chalapathi Rao N.V., Kumar A., Belyatsky B. and Lehmann B. (2018) Petrology and geochemistry of the Mesoproterozoic Vattikod lamproites, Eastern Dharwar Craton, southern India: evidence for multiple enrichment of sub-continental lithospheric mantle and links with amalgamation and break-up of the Columbia supercontinent. *Mineralogy and Petrology*, **173**, 67.

Tappe S., Foley S.F., Jenner G.A. and Kjarsgaard B.A. (2005) Integrating ultramafic lamprophyres into the IUGS classification of igneous rocks: rationale and implications. *Journal of Petrology*, **46**, 1893–1900.

Woolley A.R., Bergman S.C., Edgar A.D., Le Bas M.J., Mitchell R.H., Rock N.M.S. and Scott Smith B.H. (1996) Classification of lamprophyres, lamproites, kimberlites, and the kalsilite-, melilite and leucite-bearing rocks. *Canadian Mineralogist*, **34**, 175–186.

https://doi.org/10.1180/mgm.2022.49 Published online by Cambridge University Press